Detector simulation studies for the KM3NeT neutrino telescope

Diplomarbeit
von
Thomas Seitz

Dezember 2009

Physikalisches Institut der Universität Erlangen-Nürnberg

Contents

Part I
Introduction

The goal of this study is the evaluation of different detector designs for the new neutrino telescope in the Mediterranean, KM3NeT. For this purpose a number of different configurations for two candidate designs were simulated and the neutrino effective area as a measure of performance was calculated and compared. The compasisons were made between configurations within the same basic design as well as between these two designs. As a simulation framework the ANTARES software chain was used. This software includes gendet for the simulation of the detector geometry, i.e. the position and type of the individual photomultiplier tubes (PMTs) in the optical modules (OMs), the position of these OMs along the detction units (DUs) and the position of the DU with respect to each other (detector layout, DU distance, number, type). The genhen program was used to simulate the particles (neutrinos and muons) from non-atmospheric origin, the mupage program for those of atmospheric origin. The three parts of the km3 program suite simulated the photons generated by the propagating muons as well as the probability of a hit in the individual PMTs and to describe the detctor response (number and amplitude of hits). In the last step reco was used to reconstruct the muon track from the output of km3 (detector response) by using two different reconstruction algorithms. Calculation of the effective areas and reconstruction efficiencies was done with ROOT. During the study it became obvious that the ANTARES software is not well equipped to handle a large variation of different parameters. Many simulation parameters are hard coded and needed the recompilation not only of the used software but also of software and libraries used to compile the ANTARES software. Especially a change in the water properties requires extensive recompilation. This resulted in inconsitencies due to which the earlier simulation data was compromised and had to redone several times. Another problem is the limitation of some programs to detector size and type close to the ANTARES design, which makes extensive changes to the source code of all programs necessary for more novel design ideas like a combination of extended structures and multi-PMT optical modules. The disk space needed to store the files for the different configurations and gain enough statistics is also a limiting factor on the number of designs that can be evaluated. The study is composed of essentially three parts, the first part being an overview of neutrino astronomy and gives an answer why the building of neutrino telescopes will help to advance the understanding of the Universe. It also gives a short introduction of previous experiments focusing on ANTARES and IceCube, before describing the KM3NeT project. In the second part the focus is on the different design options, with a preference of NuONE and SeaWiet due to the above mentioned time and space constraints. The next chapters are dedicated to the software used in the study and explain how they were used and what modifications from the original versions were necessary. Finishing that part of the study is a closer look at the simulation parameters which very varied and whose effect on the detector performance was examined. The third and last part is the analysis itself. In is an extensive study into the neutrino effective area as a measure of detector performance for the different design options and their various configurations. As mentioned before only NuONE and SeaWiet options were simulated. The results for the individual options and their configurations within these options are evaluated and compared. Note that budget constraints are not

taken into consideration in this study and the only variants tested are those proposed by the respective groups that developed NuONE and SeaWiet and any change made to this designs was not done to level the playing field in terms of money. Any choice of parameters should not be interpreted as a bias towards a certain design or site. The conclusions drawn in the final chapter are based entirely on the data obtained in this study.

1 Neutrino Astronomy

In recent years, astronomy has made huge progress due to ever larger and more sophisticated telescopes. In the optical region of the electromagnetic spectrum, where adaptive optics and increasing telescope diameter, not to mention space telescopes, are the driving forces in providing mankind with ever deeper looks into the cosmos, the largest telescopes, Keck Observatory on the northern hemisphere and VLT in the south will soon be surpassed by gargantuan instruments with as much as 40m diameter in case of the E-ELT. But not only the optical part of the spectrum receives attention. The longer wavelengths have been studied by radio telescopes for decades and spaceflight has opened the way for X-ray and infrared telescopes. The highest energies are probed with gamma-ray telescopes such as H.E.S.S. and MAGIC and since recently the FERMI satellite experiment. But photons are not only cosmic messengers. It has been known for quite some time now that the cosmic rays are actually charged particles suchs as protons, electrons and heavier nuclei. The fact that these particles carry a charge and can therefore be deflected by magnetic fields limits their use since the point of origin cannot be reconstructed. Only by measuring their energies and calculating their gyro radius, it is possible to ascertain if these particles are of galactic or extra-galactic origin. But photons and cosmic rays are not the only way to probe the universe.

1.1 Neutrinos

Neutrinos have properties that make them interesting candidates for cosmic messengers: They have very small mass and interact only by means of the weak force. This means they can traverse enormous distances undisturbed because the absorption probability is extremely low and since they are neutral particles are not influenced by magnetic fields. Sources that are opaque for electromagnetic radiation can therfore be studied using neutrinos. These potential sources include Active Galactic Nuclei (AGN), Supernova remnants (SNR) and the still not fully explained Gamma Ray Bursts (GRB). In these objects protons are accelerated to energies up to $10^{20}eV$ ($10^{15}eV$ in SNR) by the first order Fermi acceleration, also known as shock acceleration. This mechanism requires the presence of a shock front which is traversed by these protons multiple times when they are deflected by magnetic irregularities on both sides of the shock front. As charged particles these high-energy protons are susceptible to loose their directional information whenever they interact with magnetic fields. However, protons accelerated by this mechanism have a high probability of interaction with surrounding protons or photons so that they can travel only a short distance from the source before the neutrino is gererated by pion-decay, thus preserving the information of the source location. These pions are generated when the protons interact with other protons or photons.

$p + \gamma/p \rightarrow N_1\pi^+ + N_2\pi^- + N_3\pi^0 + X$

About the same amount of charged and neutral pions are produced ($N_1 + N_2 \approx N_3$). The charged pions decay into neutrinos, with muons as intermediary.

$\pi^+ \rightarrow \mu^+ + \nu_\mu\mu^+ \rightarrow e^+ + \nu_e + \bar{\nu_\mu}$

$\pi^- \rightarrow \mu^- + \bar{\nu_\mu}\mu^- \rightarrow e^- + \bar{\nu_e} + \nu_\mu$

The neutral pions decay into photons allowing multi-messenger observations of the sources by using both a neutrino telescope as well as a gamma telescope.

$\pi^0 \rightarrow \gamma + \gamma$

For distances in excess of 1 kpc the ratio of $\nu_\mu : \nu_e : \nu_\tau = 2 : 1 : 0$ is changed to $1 : 1 : 1$ due to neutrino oscillation so that all types of neutrinos are available for detection. Unfortunately the same characteristics that make neutrinos excellent cosmic messengers make them very hard to detect.

1.2 Neutrino Detection Principles

Since the the neutrino is a very light, neutral lepton it is impossible to be detected directly. Furthermore even indirect detection is extremely challanging. The small cross section of interaction by neutrinos with other particles make enormous target volume a prerequisite for any attempt to detect them. Since the goal is to do neutrino astronomy it is not sufficient to use the earliest neutrino detectors, not telescopes, which were composed of a large mass of chemicals of predetermined composition. After some time the composition of the chemical was measured to calculate the number of molecules transformed by a neutrino induced reaction. Obviously no information about individual neutrinos can be gain from this methode. To get a actual telescope it is necessary to make use of the Cherenkov effect. When a charged particle travels through an insulator at speed greater than the speed of light in this medium, Cherenkov light is produced. This particles are produced by the interaction of the neutrino with the target material and has nearly the same directionality as the neutrino, provided the energy of the latter is high. To detect this light with photomultiplier tubes (PMTs), it is therefore required that the detector medium is transparent. From this light, the original neutrino energy and direction is reconstructed by measuring the distribution hits on the PMTs both in time and space and their amplitudes. Since the goal is also to look beyond our Sun as a source of neutrinos (neutrinos are produced in huge amounts by solar fusion reactions), a large volume is needed to detect the expected low fluxes. The only reasonable choices are the deep sea, beyond the reach of daylight and shielded from much of the atmospheric muon flux, and the antarctic ice.

1.3 Detection Physics

The neutrinos interact with the target material by deep inelastic scattering on the target nucleons. Depending on the neutrino flavour, different interaction types are possible. The relevant interactions for a neutrino telescope are shown below .

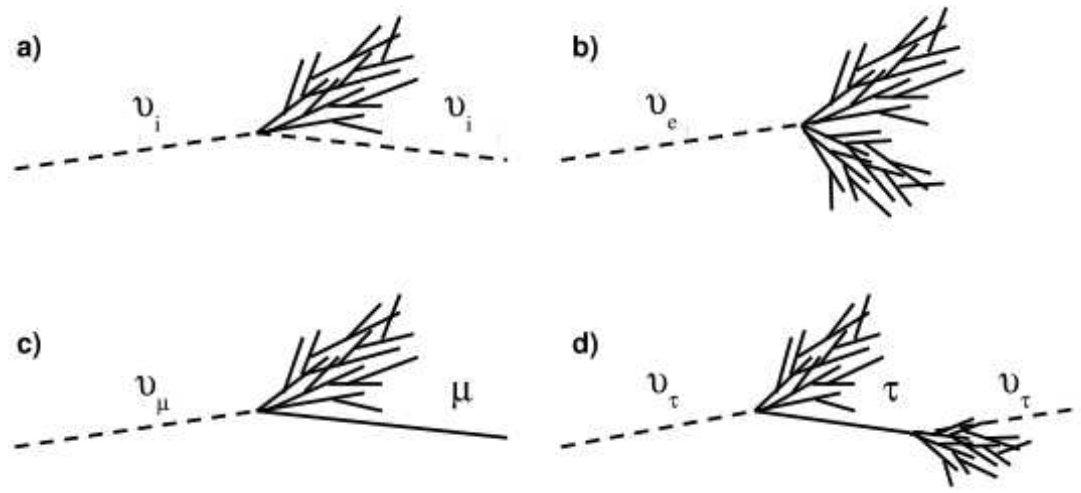

Figure 1: a) neutral-current event producing a hadronic shower; b) charged-current interaction of ν_e producing an electromagnetic and a hadronic shower; c) CC interaction of ν_μ producing muon and hadronic shower; d) CC interactionν_τ producing a τ which decays into another ν_τ creating a double-bang event signature[1]

The signature of the neutrino event in the detector can be divided into two classes and depends neutrino flavour and type of interaction, the two types being neutral-current and charged-current. These classes are either long tracks or showers. Note that both can be caused by the same neutrino. A distinction between particle and anti-particle based on the event signature is not possible. Charged-current interactions will produce both a hadronic shower and a relativistic lepton (long track).
$\nu_l + N \rightarrow l + X$
The neutral-current interaction produces a hadronic shower while the neutrino is scattered and continues its existence with a lower energy. While the charged-current interactions are obviously different for the different neutrino flavours, the neutral-current interactions are all similar.
$\nu + N \rightarrow \nu + X$
The choice reaction for a neutrino telescope is the charged-current interaction of a muon-neutrino. In this interaction a muon is produced which, travelling at relativistic speed, generates Cherenkov light along a long track. The muons of the energies interesting for neutrino astronomy loose their energy on rather slowly due to bremsstrahlung, pair production and ionisation and can last long enough before absorption to traverse a large distance. So it is possible to detect muons produced several kilometres away from the actual instrumented detector volume. These long tracks are the primary event signature for neutrino telescopes and provide a long lever arm useful for direction reconstruction.

2 Neutrino Telescopes

The following chapter provides an overview of two present neutrino telescopes. All of these telescopes work with the same basic principle, by collecting the Cherenkov light generated by the muons traversing the detection volume. They all use photomultipler tubes immersed either in water or ice. The last part looks into the KM3NeT project, for which this study was done.

2.1 IceCube

IceCube[2] is currently the largest neutrino telescope. It is the successor of the AMANDA telescope, which is located at the same site, and will be upon completion have an km^3-sized instrumented volume. As the name implies, IceCube uses ice as target material and is located at the South Pole, Antarctica. When completed, the IceCube detector will consist of 80 strings (detection units) with 60 optical modules each. The OMs contain one downward looking PMT with a 10 inch diameter, and are spaced 17m vertically. The DUs are arranged in a hexagonal layout with a DU distance of 125m. The detector is placed in the clear ice starting at a depth of 1500m and extending downward to 2500m depth. Since it is located directly at the South Pole, it is a good complementary instrument to a detector in the Northern Hemisphere.

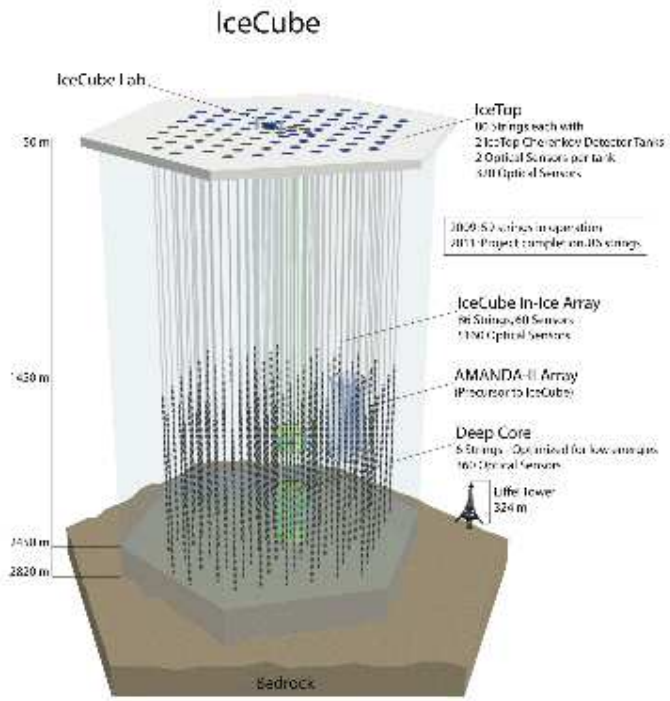

Figure 2: Schematic view of the IceCube neutrino telescope

2.2 ANTARES

The ANTARES[3] detector (Astronomy with a Neutrino Telescope and Abyss Environmental Research) is a deep sea neutrino telescope located off the French coast in the Mediterranean, about 40km away from Toulon. It is built at a depth of 2500m and consists of 12 strings with 25 storeys each. The storeys are spaced 14.5m apart and the DUs are 60 - 75m away from each other. An ANTARES storey is equipped with three OMs each housing a single 10 inch PMT looking downward at a 45° angle and are oriented at 120° with respect to each other. The electronics container on each storey houses the necessary equipment.

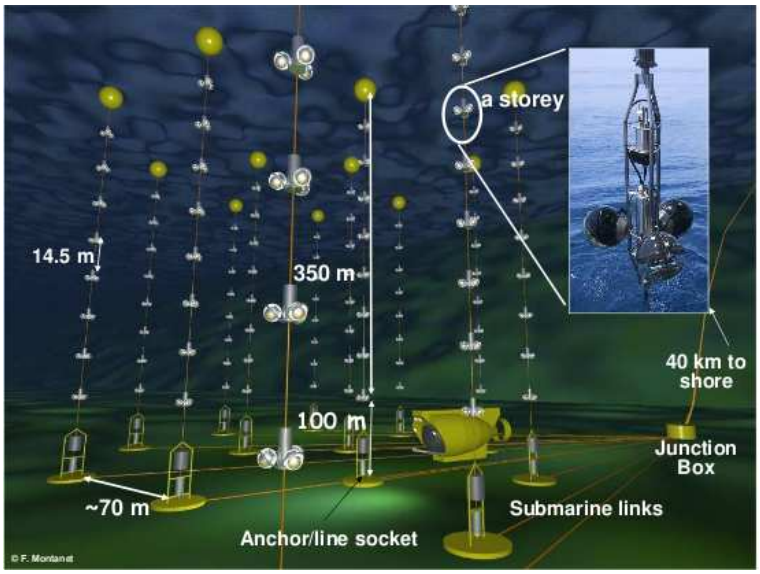

Figure 3: Schematic view of the ANTARES neutrino telescope

The detector is completed and is operational, although not to full capacity and has an instrumented volume of approximately $0.02km^2$. The ANTARES detector also serves as a test platform for accoustic neutrino detection. The software developed during the ANTARES experiment is also used for the planning of the new telescope in the Mediterranean, KM3NeT, and was used in this study.

2.3 KM3NeT

To complement the IceCube detector in the Southern Hemisphere, a km^3-sized detector in the Northern Hemisphere is necessary for a full sky coverage.

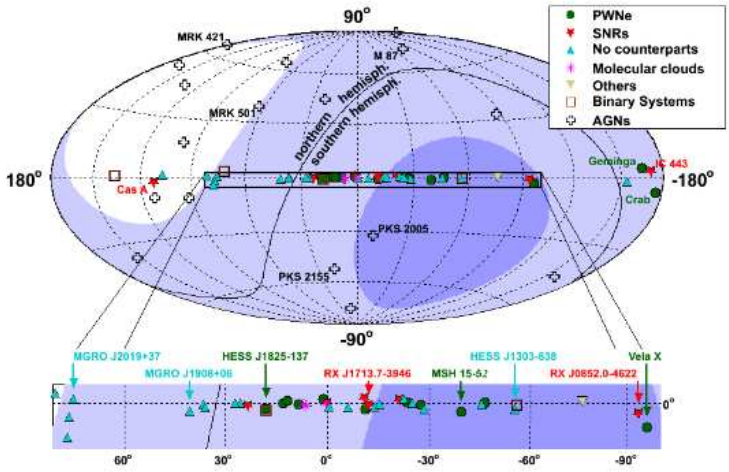

Figure 4: Sky map showing high energy γ-ray sources above 100 GeV. The shaded area (light blue: 25%, dark blue: 75% of the time) indicates the visibility for a neutrino telescope in the Mediterranean, assuming a 2π downward coverage.[4]

To achieve this goal, a new neutrino telescope in the Mediterranean has been proposed, exceedind in size the currently existing detectors, ANTARES, NEMO and NESTOR. The collaborations of these telescopes and other groups have joint to form the KM3NeT consortium and have undertaken a Design Study funded by the European Union FP6 program [5]. The consortium has prepared a Conceptual Design Report [6], outlining the basic objectives of the project. Since the publication of the CDR, the design options have been pursued further, the three candidate design are described in the next chapter. No decision on the site of the detector has been made as of the time of this study. Possible sites include the locations of the existing telescopes, ANTARES near Toulon, NEMO near Capo Passero off the coast of Sicily and NESTOR of the Greek coast near Pylos.

The final design was also not yet fixed, allowing for additional analysis of the different configuration, as was done in this study. Three designs were developed and the final recommenation of the design will be made in the Technical Design Report (TDR), early in 2010.

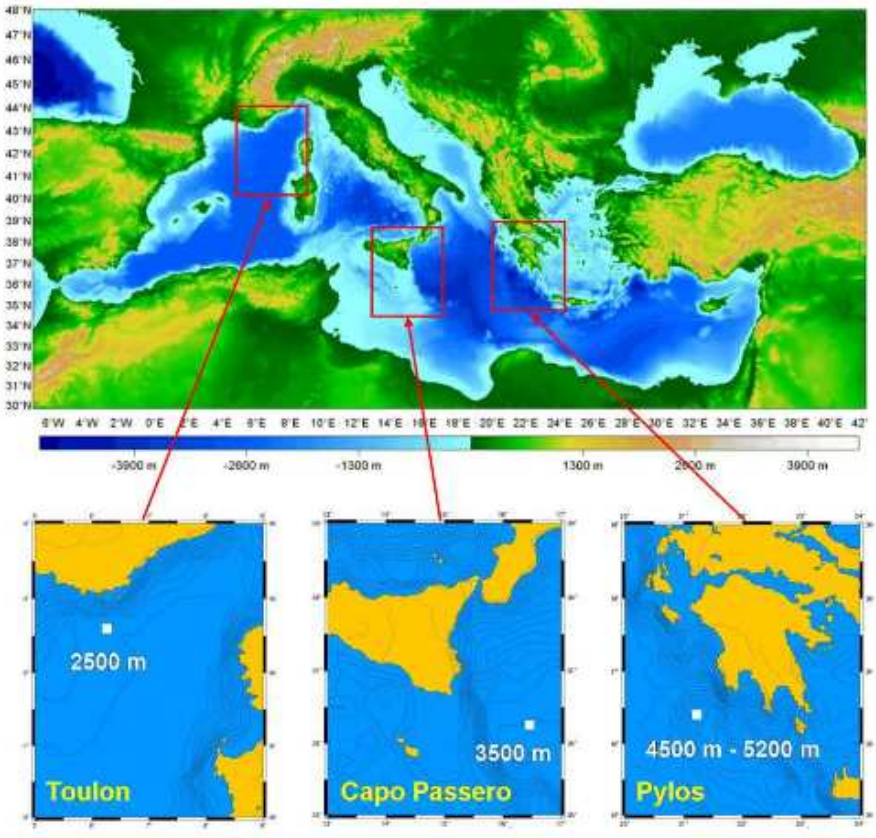

Figure 5: Potential sites for the KM3NeT neutrino telescope

3 The Design Options

This section describes the design options under consideration for the KM3NeT telescope. Any description provided here was current at the time the simulations were performed and may have become outdated later. The descriptions are only concerned with the detector properties such as choice of PMTs, storey design and layout of the whole detector. Data taking and processing and other technical details like deployment are neglected here since they are not relevant to the study.

3.1 NuONE

The NuONE[7] design (also νONE) uses a semi-rigid system for its detection units, which will also be referred to as towers in contrast to strings. Each detection unit (DU) consists of 20 storeys (bars) which host three groups of two photomultipliers, a total of 120 per DU. Vertical spacing is 40m between storeys, yielding a total height of 860m for the DUs. The storeys are connected with tensioning ropes to force each storey to a perpendicular orientation with respect to its vertical neighbours.

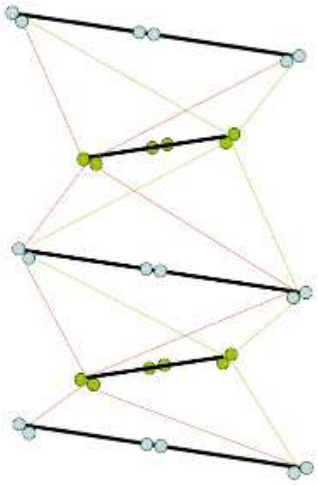

Figure 6: Schematic view of a NuONE detection unit

The layout on the seabed is a hexagon in which the DUs are 180m apart. A total of 127 DUs make up the detector. In this study the DU distance was also set to 130m and the number of DUs to 154 to examine the effect of these changes on the performance of the detector. The storey layout was fixed for this study at a bar length of 8m and the PMT size was chosen at 8 inch (standard) or 10 inch. As for the orientation of the PMTs, the outer pair consists of one PMT looking outward and one PMT looking downward, with the third pair sitting at the centre of the storey with both PMT looking downward at 45°.

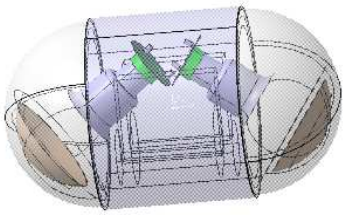

Figure 7: Schematic view of the NuONE optical module containing two PMTs

This design is based on [7] with the only difference in using the 8m bar length proposed in an earlier draft.

3.2 SeaWiet

SeaWiet[8] is an acronym for SEnsor Architecture for a WIde Energy range Telescope. This design features multi-PMT optical modules with 31 3-inch PMTs each and one OM per storey. Originally, this design option provided for a 300 DU detector with an octogonal layout on the seafloor.

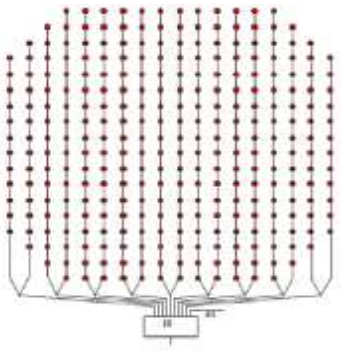

Figure 8: Octogonal layout for the 300 string version of SeaWiet

As with NuONE the design calls for 20 storeys per detection unit. The distance between storeys was set to 30m and the spacing between DUs to 130m. Both of these parameters were varied in this study. Later a detector with 310 strings in a hexagonal layout was proposed, which is also included in this study. The detection units feature storeys that are made up of only the optical module with no other structural extensions. These OMs contain the 31 PMTs, 19 of which are located in the lower hemisphere of the OM, 12 in the upper one.

Figure 9: A SeaWiet multi-PMT optical module

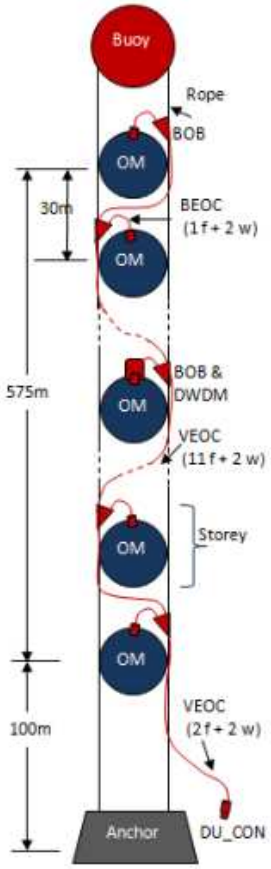

Figure 10: Schematic view of a SeaWiet detection unit

Inquiries were also made in the use of Winston cones to increase the collection area of the PMTs [9] but were not incorporated into this analysis. The description originally called for the use of 42% qe PMTs, but since none were available at the time of this study, the same quantum efficiency (35%) was used as for the PMT in the NuONE design. Other than that the simulated detector design follows the one outlined in [8].

3.3 MEDUSA

MEDUSA[10], MEDiterranean Undersea String Architecture, is described as a set of technological solutions rather than a comprehensive detector design . A hexagonal layout was proposed but without any fixed number of DUs or distance between DUs. For the detection units, a vertical spacing of 30m between storeys is proposed.

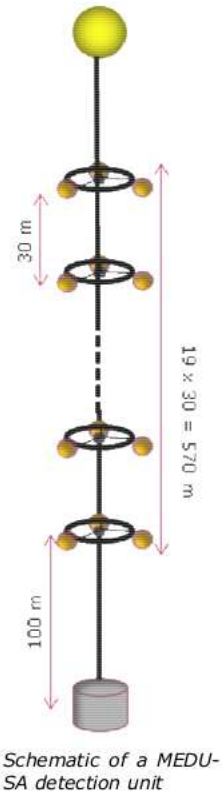

Figure 11: Schematic view of a MEDUSA detection unit

The optical modules, three per storey, in this proposal are 40cm away from the axis of the line and will house one PMT looking 45° downward. The PMT is contained in a 17-inch glass sphere, the same used for ANTARES.

The size of the PMT is not specified, but can be chosen between 8 inch and 10 inch. During the Design Study, support for MEDUSA gradually declined as the focus of interest shifted to NuONE and SeaWiet. To be able to simulate more design configurations for this study, it was decided not to incorporate any MEDUSA configuration.

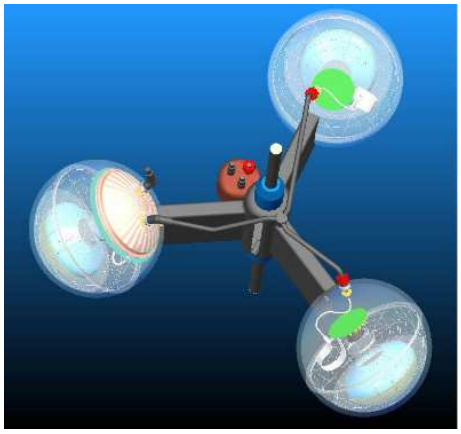

Figure 12: A MEDUSA storey

4 The Software Chain

The software used in this study is commonly referred to as the ANTARES software chain. The name ANTARES is an obvious reference to the telescope project during which the individual programs were designed. Chain refers to the successive use of the different programs on the output of the previous program as a input of the next one. This study was limited to the use of the core of the software chain and so only these will be described. All the programs require the use of separate sub-programs from which subroutines are incorporated into the program during compilation. These sub-programs are not explicitly described although they are vital to the fuctioning of the programs, since they were not modified in the scope of this study. For this analysis only the finished programs were used although modification of their proper source code was necessary.

4.1 Gendet

The gendet program creates from a user input in the form of an ASCII file with the basic detector parameters another ASCII file as an output. This output is used to describe the detector, i.e. the position of every single photomultiplier, to the subsequently used programs. In this study, only the most basic function of the program was used to produce a detector file which includes only type and position of the PMTs. Additional features include the stretching of the lines due to pull of the top buoy and the possibility to apply a constant water current. This would require a more detailed knowledge of the material properties of the used detector. As a default option the properties of the components of the ANTARES detector are included in the software. Since these properties only affect the more advanced features of the program, which were not used in this simulation, the use of these wrong properties has no effect on the produced detector file. A more serious issue is the limitation to string designs, one design for all detection units and one storey design. To simulate NuONE storeys, which are extended and perpendicularly oriented towards each other, a workaround was used by traeting two neighbouring storeys as one storey carrying twice the number of PMTs. Even at this early stage in the simulation process, the input of the PMT properties, diameter and transit time spread (TTS), is necessary. For a more detailed description see [11].

4.2 Genhen

For the production of all particles to potentially reach the detector, the genhen program is used. This program is part of the genneu software package, whose other parts were not used in this study. Genhen produces neutrinos with preselected properties such as flux, energy and flavour as well as the neutrino direction, which is sampled isotropically within a predefined range of nadir angle. For a lack of a better term, this last property is call angular distribution in the rest of this analysis. In this study only muon neutrinos were simulated, so genehen also produces the secondary muons and propagates them to the detector, also calculating their energy loss according to the surrounding medium (rock or water/ice). The detector is contained in a can which is simulated by the software. This can volume is a cylindrical volume extending from the detector by a predetermined radius, usually measured in units of maximum absorption length.

In this simulation, this radius was defined as three times maximum absorption length and varies therefore with the used water model. Beyond that can volume a generation volume is simulated, extending from the detector by the maximum muon range, limited in the z-direction by the sea surface. To simulate the neutrino interactions the program uses both LEPTO and RSQ, for which different Parton distribution functions are available. For muon neutrinos with the vertex outside the can, the program uses MUSIC, MUM or PropMu for propagation. These propagation codes fail for energies higher than $10^8 GeV$, so this sets an effective upper limit for the neutrino energy. This means that the simulation of GZK neutrinos, the cosmogenic neutrino flux is not possible with genhen, since these neutrinos are expected to have energies as high as $10^{11} GeV$. For further information see [12].

4.3 Km3

The event files (ASCII) produced by genhen serve as input in the km3mc part of the km3 program package. The km3 package consists of three programs, gen, hit and km3. All three are necessary to perform a detector simulation. This software is used to calculate the detector response caused by the muons simulated with genhen or mupage (mupage is treated later). The gen program is used to simulate the photons generated by a certain length of muon track or secondary electromagnetic shower. Around this part of the track, a number of concentric shells are produced at predefined distances. All photons reaching each of the spheres are stored using a GEANT simulation. This includes scattered photons and the output is a number of files which will serve as input for the hit program. The program gen requires the water properties of the simulated site. This includes absorption and scattering lengths and a water model describing the interactions between the water and the photons. For each investigated water type, a new set of files must be produced.

As the next step, the hit program uses these output files (one for muons, four for showers) to calculate the hit probability in the PMTs, which are then stored in tables. In order to do this, all PMT properties must be changed in the code itself (hit-ini-optic.f) every time the PMT type is changed and new tables (hit output) must be produced accordingly. The properties necessary for the calculation of the hit probabilities include the quantum efficiency and angular acceptance but also the transmissivity of the glass sphere and the gel used for storing the PMT in the storey.

The output of hit (tables) are then used as input in the km3mc program, which does the actual simulation of the detector response. The muons are propagated through the surrounding medium with MUSIC and the information of the track is used in conjunction with the hit tables to determine the hits in each individual PMT. At this stage ^{40}K background can be added by an input of the rate per PMT. The output of the km3 program is again an ASCII file which can now be used in the reco software. A description can be found in [13].

The km3 package can be considered the heart of the software chain. Here the environmental parameters and the PMT properties can be varied, which is necessary to simulated different sites and different photomultipliers. However since all of these properties are buried in the code itself, it requires a good knowledge of the program source code to successfully apply any changes. A great deal of problems can arise when consistency between all parts of the software chain is not strictly observed or when one place where such a modification would be necessary is overlook. Over the course of this study, both errors were made and the correction required a lot of time.

4.4 Reco

Finally, the output from km3 can be used for reconstruction with the reco program. The reco program allows the use of different reconstruction strategies (algorithms), of which only the Aart Strategy (aart) and a modification of this strategy (zmod) were used. The reconstruction of the muon track, and thereby implicitly the neutrino track, is basically the same for both algorithms. After applying a first geometric fit whose result is used as a starting point the next fit (maximum likelihood) and so on until a final fit is produced. Each fit is tested for compatibility with the track used as starting point. A detailed description of the reco algorithm is found at [14] for aart and [15] for zmod.

4.5 Mupage

Mupage[16] is used to simulate atmospheric muons. The number of the muons can be set by the user and instead of the detector file a parameter file with the can size of the detector has to be used. The can size can be found all event files produced by genhen or subsequentialy produced by km3 or reco. The specifics of the detector are not needed, only the depth in the sea. The output from mupage can then be further used in km3 and reco. Since the study of the atmospheric muon background was only a side note in this analysis, the amount of simulations produced is very limited.

Part II
The Analysis

The main part of this study is the analysis of the various detector design configurations and their performance in terms of neutrino effective area and reconstruction efficiency, both of which will be defined below. This analysis not only examines the performance of detector configurations within one type of design (NuONE or SeaWiet) to determine the effect of the variation a single simulation parameter. Beyond this study into the optimisation of the design types, the comparison between the two different design types is also part of this analysis. Since it became clear during the KM3NeT Design Study that the main contenders are SeaWiet and NuONE, the MEDUSA design was not incorporated into this study to allow more variations of the two other designs. While the water properties, absorption length, scattering length and to a smaller effect ^{40}K background rate, are environmental properties and therefore are part of the site consideration for all types of detectors, it was included separately for both designs to highlight any differences in the impact of these parameters for the individual design. The same is true for the analysis of the effect of depth on the atmospheric muon background, which was performed only for one SeaWiet configuration because of the resource-intensive nature of these simulations. The performance analysis also includes a study of the effects of a changing of the angular distribution of the neutrinos generated by the genhen program. Obviously it is not possible to build a detector that is only sensitive to either up or down-going neutrinos, although it is possible for a design to be strongly biased towards one distribution. During this study it became clear that one reason of the differences in effective area estimations from different groups were the different angular distributions chosen. To estimate this effect it was included in this analysis and allow a superficial comparison. This is not a substitute for a simulation with the same angular distribution of generated neutrinos and should be used as a rule of thumb only. The reconstruction algorithm used in the reco program is also neither a design nor an environmental parameter. Its variation can also be used when comparing different simulations, in this case by comparing simulations of the same design but using different reconstruction strategies. The performance analysis is devided between the two design types, NuONE and SeaWiet. Both parts are summarized and followed by a quick look at the proposed doubling of the detectors and finally a comparison of the two design types.

5 The Simulation Parameters

As simulation parameters this study considers environmental parameters such as water properties as well all other design parameters. Although not a simulation parameter in the above defined sense, the statistical considerations and the influence of the reco algorithm in general are included in this chapter.

5.1 Statistics

As with all Monte Carlo simulations it is important to produce enough events so that statistical variantions cancel out each other and the final data becomes reliable. Since both disk space and CPU time are limited compromises cannot be avoided. Due to the number of different configurations simulated and the fact that other people are also in need of disk space for their own simulations, an upper limit on the number of simulated events had to be obeyed. This limit is not a strict one and the different detector configurations were simulated with different number of events. As a result some simulations show less statistical variations than others but it was assured that for every generated event a different random seed input was used. The number of simulated neutrinos is in every case at least 10^8 which yields a corresponding number of muon events in the range of 10^5. To closer investigate this problem, a number of simulations to measure effective area were compared to each other for two different design options. The first plot shows the ratios of six measurements to one baseline for the SeaWiet design with 310 strings, hexagonal layout and 2π angular distribution of generated neutrinos. The greatest statistical variations are for energies below $10^4 GeV$ and above $10^6 GeV$ with differences in individual bins of as high as 30%. In the intermediate range between $10^4 GeV$ and $10^6 GeV$ the differences are usually below 10%. The different results for different energy ranges can be explained by the fact that in these parts of the energy spectrum only a small number of events can be reconstructed (low energies) and in case of the highest energies only comparably few events were generated to begin with due to lower flux.

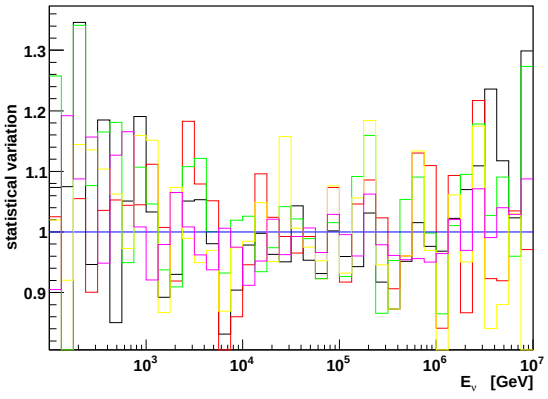

Figure 13: Statistical variation between different simulations of effective areas (SeaWiet_310hex40_130)

A similar picture emerges when examining the NuONE detector design, using nine simulations for the standard design option and assuming 4π angular distribution, while using the same environmental parameters and the same reco algorithm (zmod) as for the SeaWiet simulation above. However, the differences are generally larger than in the case of the SeaWiet design. The differences in the low energy range below $10^4 GeV$ are especially pronounced with individual bin differences of more than 100%. In the energy range above $10^4 GeV$ there are no further discernable divisions in the energy spectrum

as with the SeaWiet case. For energies higher than $10^4 GeV$ the differences are around 20%. The more pronounced statistical variations in the lower energy range compared to SeaWiet is due to the generally lower reconstruction ability of the NuONE design with its larger distances between detection units. This reduced reconstruction capability is also responsible for the greater statistical variations in the energy spectrum above $10^4 GeV$ by reducing the number of reconstructed events.

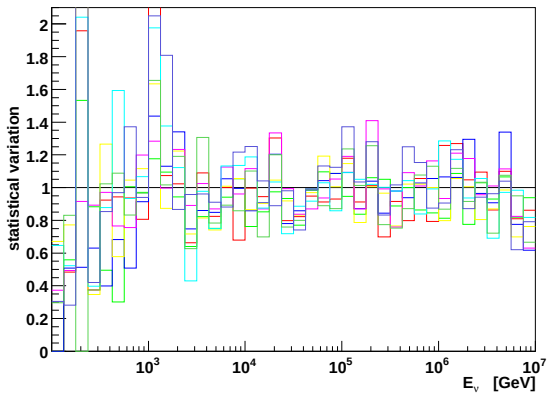

Figure 14: Statistical variation between different simulations of effective areas (nuOne8_180m8)

Although the differences for individual bins can be quite large when comparing two diffrent simulation results, it can be seen that there is no continuous trend it these differences, no measurement is higher across the entire energy spectrum. There are usually no more than three neighbouring bins either higher or lower than their corresponding parts. That means that when comparing two different design options and their histograms are continuously different from each other over parts of the energy spectrum, it is very unlikely that this is merely the result of statistical variation. At least a general trend can be retrieved from such comparisons even when the differences are small as long as these differences resist continuously over several bins, although the size of the difference cannot be precisly determined. This is especially true for the NuONE design configurations and for all simulations using the original Aart Strategy (aart) as can be seen in the plots below.

For the SeaWiet design, here with 300 strings and 4π angular distribution, the statistical variations are greater when using the aart reco algorithm than when using zmod, particularly in the lower energy range. Here the Aart Strategy performs worse than zmod, i.e. reconstructs less events, so the lower number of events allows for greater relative variations. In the case of the NuONE design the effect is very similar for both reconstruction strategies. As an outcome of these comparison is must be conceded that for low energies the individual analyses will provide qualitative rather than quantitative results. Bearing this in mind it was decided that the preference for a greater number of different detector configurations over better statistics for fewer designs was justified. When the number

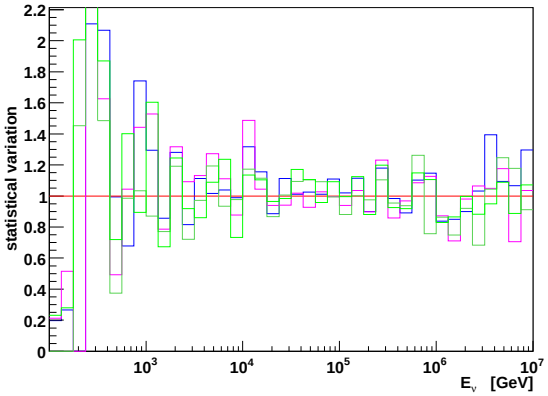

Figure 15: Statistical variation between different simulations of effective areas (SeaWiet_300oct_130), aart

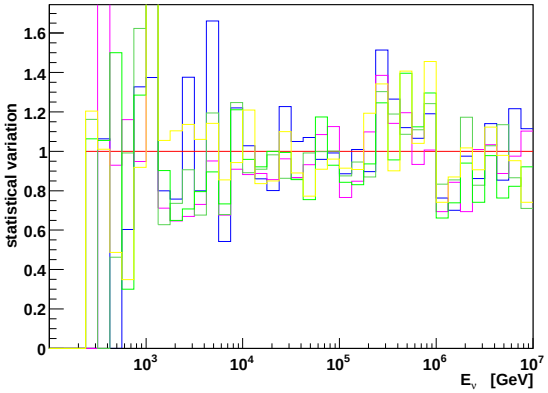

Figure 16: Statistical variation between different simulations of effective areas (nuOne8_180m8), aart

of different design options has been narrowed down it can still be considered to increase the number of simulated events by one or two orders of magnitude per design which will correspond to 30 - 300 files (genhen + km3 + reco) with a total of about 1TB each if all the files are kept, 10 - 100 files with around 300GB for just the reco files. For the mupage simulations a similar concern about disk space lead to the decision to limit the number of files, since a file containing one million events (288s livetime) for the SeaWiet design exceeds 50 GB when processed with the km3 program.

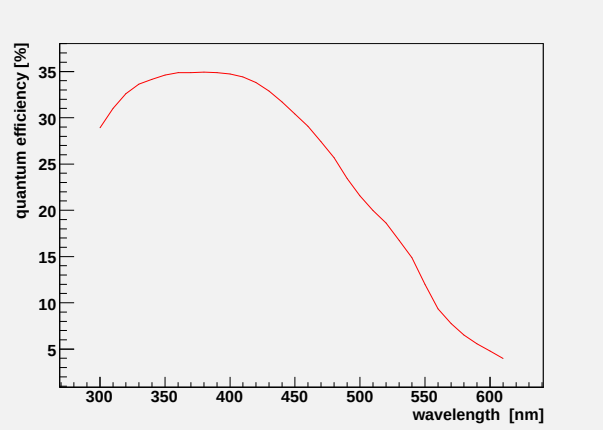

Figure 17: quantum efficiency for all used PMTs

5.2 PMT Properties

For the simulation of the photomultiplier tubes in the individual designs, it was chosen to depart from the write-up proposals. Originally the SeaWiet optical module was planned to be outfitted with high-qe PMTs with a maximum quantum efficiency of 42%. However, during the Design Study, it became obvious that no such photomultiplier is currently built by any manufacturer and after the Photonis corporation ceased the production of PMTs no such high-qe PMT is to be expected in the foreseeable future. For this reason it was decided to use one model of PMT for both NuONE and SeaWiet in this study with the only difference being the photocathode area. Another point of departure from the original design for SeaWiet is the use of a flat photocathode instead of the proposed curved one, so for the simulation angular acceptance is $\cos\theta$ for all designs. The Winston cone modification for SeaWiet to increase the photosensitive area has also not been implemented for the yet unknown change in angular acceptance. All other properties of the PMTs used (TTS, dynode structure, electronics) come from the code of the software chain (hit-ini-optic.f in the hit part of the km3 package) and are those of an ANTARES Photomultiplier. The same is also done for all non-PMT storey properties such as the optical properties of the glass sphere and the gel between glass and photocathode (also from hit-ini-optic.f). The quantum efficiency for the PMTs is taken once more from the code of hit-ini-optic.f and has a maximum quantum efficiency of 35%.

Measurements performed at ECAP have shown that this is a reasonable value that can be expected from the latest ultra-bialkali photocathodes currently in production. Once the photomultiplier tubes for the respective designs have been selected further simulations can be performed. Unless the PMTs will be radically different from the simulated model the effective area can be expected to scale approximately with the quantum efficiency. One proposed PMT prototype for the SeaWiet OM features a quantum efficiency curve with a maximum at a different wavelength which would require additional simulations because of the multiple effects that prohibit a simple estimation. Any changes in quantum efficiency will also affect the rate of ^{40}K induced optical background.

5.3 Water Properties

The detector medium for KM3NeT will be water so it is only natural that the water properties are important parameters in the simulation. Since the site for the detector has not yet been selected it is not possible to use any actual data. However, from previous measurements e.g. at the ANTARES site, an artificial water model can be implemented in the simulation. Several such models exist and are used in detector simulations. Examples for such models are NEMO and ANTARES-Smith-Baker which describe the absorption length with respect to the wavelength of the photon. For this study, two different water models were used, based on but not identical to the models mentioned above, called 'nemo' and 'asbw' after their sources of inspiration.

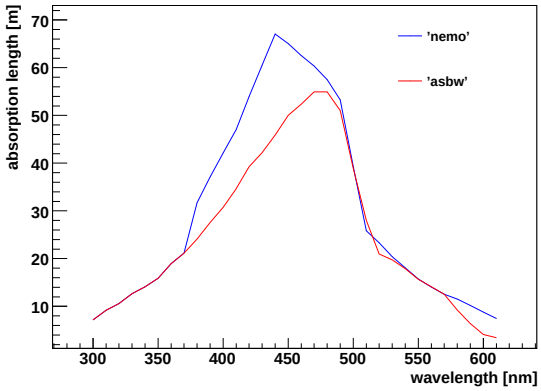

Figure 18: absorption lengths for the two water models

The fact that unofficial water models have been used makes the comparison with different simulations performed by others more difficult. But since the values for the absorption lengths for the NEMO water were in the wrong part of the spectrum for the used software, it was inevitable that some differences would occur. The asbw water properties come once more from the source code of the km3 package, the nemo water uses the official NEMO absorption lengths in the part of the spectrum compatible with km3 and uses the values from asbw in the other part. Since the drop in absorption length is rather sharp when moving from NEMO to asbw it can be assumed that the values for this part of the spectrum are underestimated. Scattering lengths are usually not defined for these models so one set of values found in the source code for the km3 package were used for both water types which renders the simulaton a little unrealistic since it can be expected that scattering length changes for different absorption lengths.

The implementaion of different water models requires both user input at all stages of the software chain as well as recompilation of the hit part of the km3 package. After the recompilation, new photon tables have to be produced with the gen and hit parts.

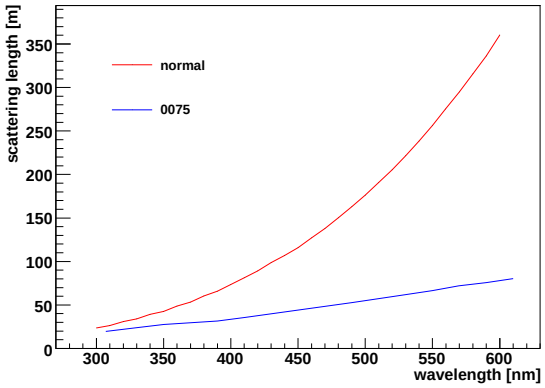

Figure 19: scattering lengths for the two different options

To be on the safe side the software chain (genhen, km3) has been recompiled for both water models to ensure consistency. Since the water properties are also hard coded in the geasim program and library, they have been recompiled as well anlong with genhen which uses libgeasim for compilation. Furthermore the maximum absorption length is used to calculate the can size in genhen (user input) and therefore implicitly in mupage and is also required in the parameter file used for reco. This extensive procedure is one of the major drawbacks in the software chain. Failed compilations and forgotten value changes are the cause of the corruption of earlier data which rendered the results incomparable to other simulations due to internal inconsistence with regards to the correct absorption lengths.

5.4 Background

As stated previously two kinds of background are important for neutrino telescopes, bioluminesence and Cherenkov light from ^{40}K-decays. The bioluminesence background has been neglected in this study because there is no possibility to include bioluminesence in the ANTARES software chain without an extensive rewrite of both km3 and reco. Furthermore, since the site for the detector is not yet selected, there are no measurments yet for all possible sites which incorporate seasonal variations. For the ^{40}K background it was assumed that the concentration of ^{40}K is the same for both water models and all sites and therfore the background rate is also constant for all cases. The rate of background was calculated using

$R = 364Hz \times A(cm^2) \times qe$

,where A is the photocathode area in cm^2 and qe the maximum quantum efficieny [17].

^{40}K background rate:	
8 inch PMT	41315 Hz
10 inch PMT	64555 Hz
3 inch PMT	5819 Hz

5.5 Reco Algorithms

The software used for reconstruction of events, reco, allows for the application of two different reconstruction algorithms. The first one is the original Aart Strategy of which a detailed description can be found in [14]. This reco algorithm will be called aart in this study. Zmod, the second algorithm, is actually not a completely different strategy but a modified version of the Aart Strategy, based on suggestions by D. Zaborov. These modifications were implemented to increase the reconstruction capability for larger detectors. Another modification concerns the thresholds that need to be exceeded in order for a hit to be reconstructed instead of rejected. To allow for the reconstruction of a larger fraction of hits these thresholds were lowered. A detailed study of this modifications and a comparison with the original Aart Strategy can be found in [15]. To evaluate the two strategies, a simple detector design was chosen. It consists of 25 strings in a square 5×5 layout and features 10 ANTARES storeys with three optical modules per string. Each OM consists of one 10-inch Photomultiplier with the standard quantum efficiency of 35% used in this study. The simulation was performed only with nemo water and an angular distribution of 2π. As a measure of performance the neutrino effective area was used to compare the two strategies.

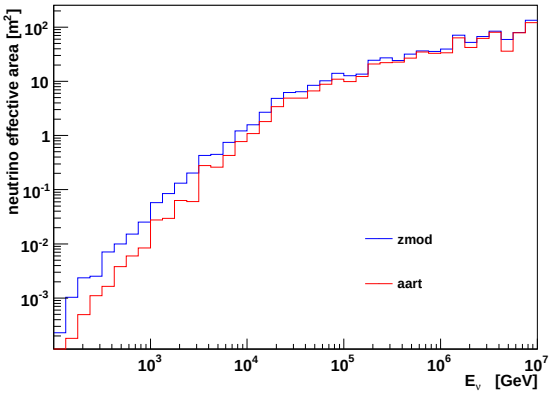

Figure 20: Comparison of the effective areas for the test detector

The zmod strategy performs better across the whole energy spectrum with the highest increase over aart at energies below 10 TeV. Above 10 TeV the difference between the two strategies declines but zmod still yields a 5 - 10% higher effective area. It has to be noted however that due to low statistics these values are not very precise.

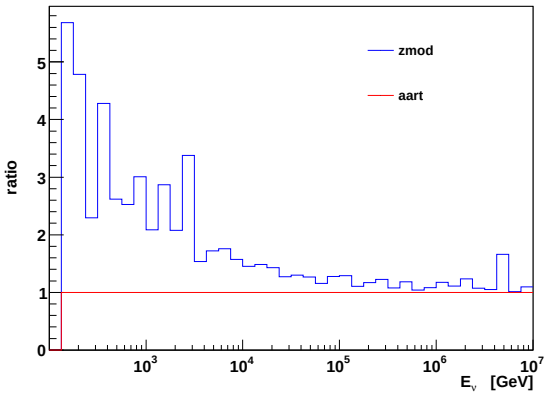

Figure 21: Ratios of the effective areas for the test detector

6 Performance Analysis

For the evaluation of the design configurations, the neutrino effective area and the reconstruction efficiency were chosen as measures of performance. In this part of the study a number of different design options for both NuONE and SeaWiet are investigated with the use of Monte Carlo simulations. The results are shown in plots which compare both absolute values as well as ratios of these values for the different configurations. In some plots the name of the design configuration used internally in this study was used to indicate the chosen option. For these the following nomenclature was used to identify the specific design: the NuONE detectors are called:

nuOne(bar length)_(DU distance)m(PMT diameter in inch)

The SeaWiet detectors are:

SeaWiet_(number of DUs)(geometry)(storey distance, only when 40m)_(DU distance)

6.1 Neutrino Effective Area

An important parameter to measure the performance of a neutrino telescope is the neutrino effective area. This effective area depends on several factors independent of the detector (physical constants) and the effective volume, which depends on the efficiency of the detector. The neutrino effective area is defined as

$A_{eff}(E_\nu, \theta_\nu, \phi_\nu) = V_{eff}(E_\nu, \theta_\nu, \phi_\nu)(_A)\sigma(E_\nu)P_{Earth}(E_\nu, \theta_\nu)$

The effective volume is given by

$V_{eff}(E_\nu, \theta_\nu) = \frac{N_x(E_\nu, \theta_\nu)}{N_{gen}(E_\nu, \theta_\nu)} V_{gen}$

V_{gen} is the generation volume where the events, in this case muons, are produced and extends far beyond the can volume depending on the neutrino energy (see [12]).The generation volume is calculated from the center of the detector (c.o.g.) and not from the edge as the can volume is. Therefore a larger detector will have a higher effective volume and thus a larger effective area. N is the number of reconstructed events and N_{gen} is the number of generated events so that N/N_{gen} is the reconstruction efficiency of the detector. The detector-independent parameters include the target nucleon density $(_A)$, the neutrino-nuleon cross section $\sigma(E_\nu)$ and the probability for absorption in the earth P_{earth}. This probability is defined as

$P_{Earth}(E_\nu, \theta_\nu) = e^{-N_A \sigma(E_\nu) \int \rho dl}$

where $\int \rho dl$ is the integrated density along the direction of the neutrino track and $\sigma(E_\nu)$ is again the neutrino-nucleon cross section. Although the effective volume alone would also be a good candidate for measuring detector performance since it contains the reconstruction efficiency which, apart from the angular resolution, is the most important property of a neutrino telescope, it is customary to calculate the neutrino effective area and then compare different designs. The following chapter will detail the effect of different parameters on the performance of the NuONE and SeaWiet detector designs.

6.2 Results for NuONE

For the NuONE design option seven parameters were varied and the effects of these variations on the neutrino effective area was analysed. The design parameters storey distance, number of storeys and the horizontal extension of the storeys (bar length) were kept constant. Since the gendet software does not permit different storey configurations it was necessary to simulate a double-sized storey containing 12 PMTs instead of six, with a vertical expansion of 40m. It is not known if this workaround produces any peculiarities but so far all results are comparable to the results of other groups involved in the simulation of this design. The first part will deal with the effective area of the various design variations, followed by a closer look at the reconstruction efficiency and the effect of atmospheric muons with respect to two different depths.

6.2.1 Effective Area

The first variation concerns the angular distribution of the generated neutrinos. 4π means an isotropic distribution of both up-going and down-going neutrinos, 2π an isotropic distribution of only up-going neutrinos. The results show a marked difference between the calculated effective areas in the the two cases. While in the case of 2π angular distribution the effective area reaches a maximum of around $750m^2$, it reaches more than double that for an angular distribution of 4π. Additionally one can see a clear excess of effective area in the energy range below $3 \times 10^5 GeV$ for the 2π angular distribution, reaching 4 times as high as in the 2π case for low energies and stays at 2 - 1.5 times the value for 4π until $10^5 GeV$. This clearly shows the importance of being consistant when comparing different results. The simulation was performed using nemo water and the zmod reconstruction strategy for the standard 8-inch PMT.

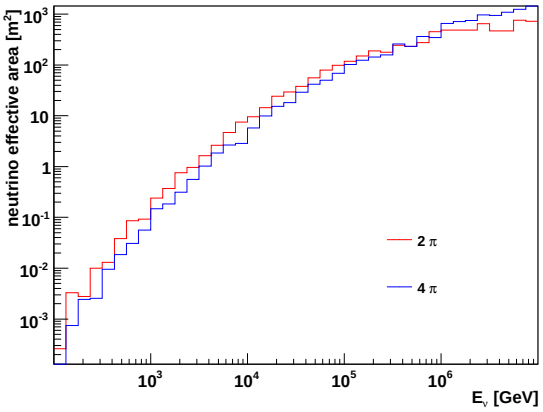

Figure 22: comparison of effective areas

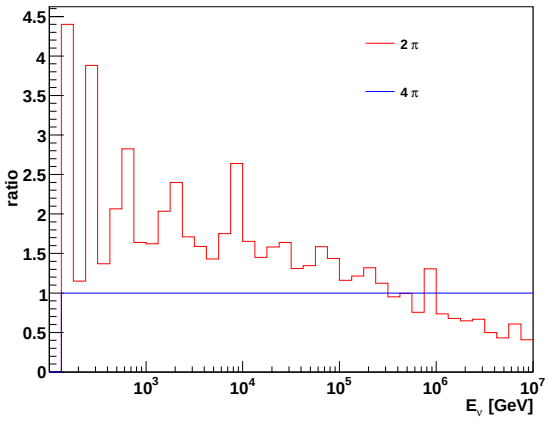

Figure 23: ratio of effective areas

Earlier in the Design Study the size of the photomultipliers to be used in the storeys was not fixed to 8 inch. Another possibility was the use of 10-inch PMTs (same size as in ANTARES). The increase in photocathode area from the 8 inch to the 10-inch PMTs is 56%. For energies above $10^6 GeV$ to effective areas are roughly the same for the both PMT sizes. The increase in effective area starts with a factor of ca. 4 and levels off between 10^4 and $10^6 GeV$ at 30%. A similar increase in neutrino effective area is expected for the other designs as well if the photocathode area is increased. The higher the expected neutrino energies are the smaller the gain will be. This simulation was performed only for a 4π angular distribution of generated neutrinos using nemo water and the zmod strategy.

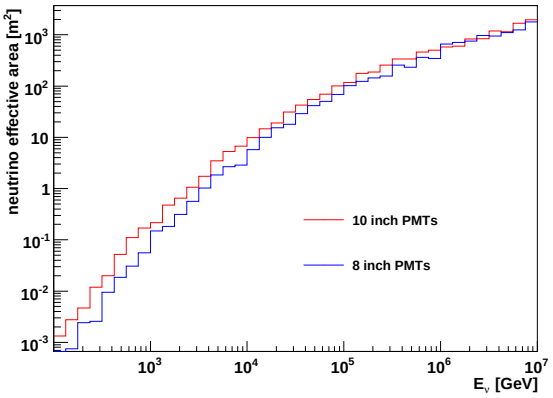

Figure 24: comparison of effective areas

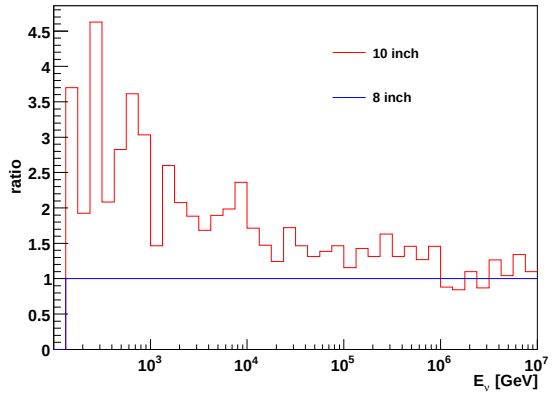

Figure 25: ratio of effective areas

Two different water properties have been studied, absorption length with respect to the photon wavelength and scattering length, also dependent on the wavelength of the photon. Again it has to be emphasised that the two water models do not correspond to any of the proposed sites. The different absoption lengths were studied for the design with

the 8-inch PMTs and angular distribution of 4π. It is clearly seen in the ratio plot as well the comparison plot that the effective area is higher for the nemo water across the whole simulated energy range. The increase is highest in the energy range up to $5 \times 10^4 GeV$ with on average 40% and is going to 20% until $10^6 GeV$. The increase levels off at around 10% for energies beyond $10^6 GeV$. This shows a nearly linear influence of the absorption length, which is in this case 20% higher at the maximum for the nemo water compared to the asbw water, on the effective area. That the increase is more pronounced in the lower energies than the higher range is due to the fact that with this increase in absorption length it is possible for more Cherenkov photons to reach a PMT to cause more hits or hits with a higher amplitude beyond the energy threshold of the reco strategy. So otherwise rejected events can be reconstructed. For higher energies the effect is smaller since such events produced usually a high enough number of hits anyway to allow for reconstruction.

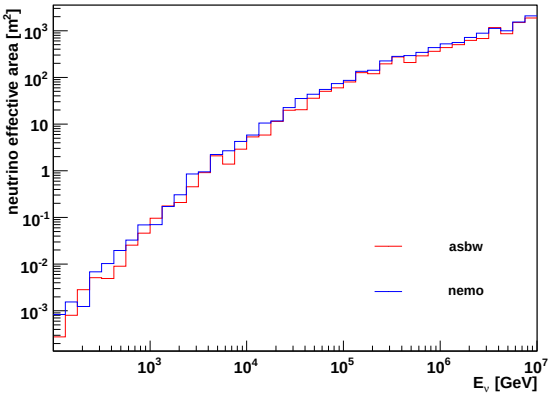

Figure 26: comparison of effective areas

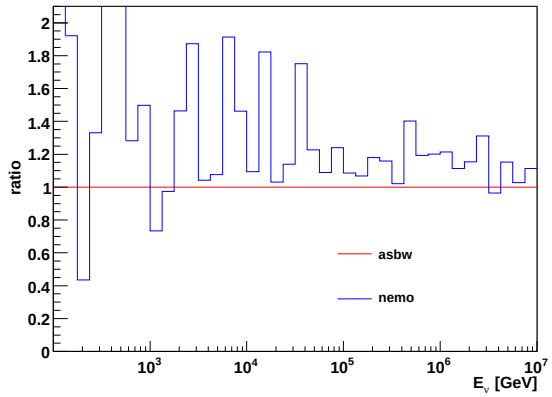

Figure 27: ratio of effective areas

While the basic hexagonal layout of the nuOne design option was left unchanged, the distance of the detection units was varied to study the effects of a different instrumented

volume and of a different instrumentation density on the effective area. The results two effects for an increase of DU distance from 130m to 180m. Below $10^4 GeV$ the effective area is smaller for the larger DU distance for as much as 40% around an energy of $10^3 GeV$. Above 10 TeV the effective area for the 180m distance increases beyond that of the 130m DU distance and reaches on average 150% compared to the smaller one with a maximum of 200% in the last energy bin at $10^7 GeV$. The increase in effective area for the 130m DU distance geometry can be explained similarly to the increase for the larger absorption length in the previous paragraph. Low energy photons (<10 TeV) have a higher probability to reach more PMTs if the detection units are closer together. For higher energies the larger detection volume dominates the effective area which becomes highest in the last energy bin where the twofold increase closely matches the 1.9 times increase in detector surface area.

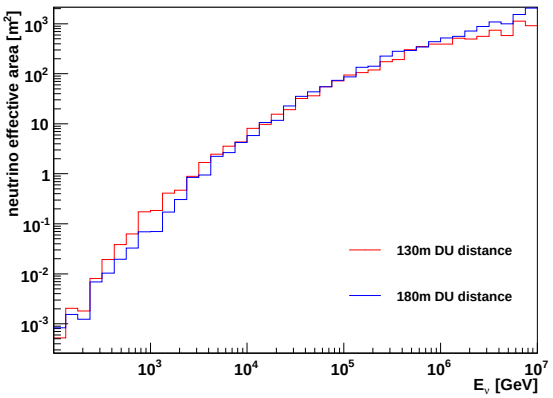

Figure 28: comparison of effective areas

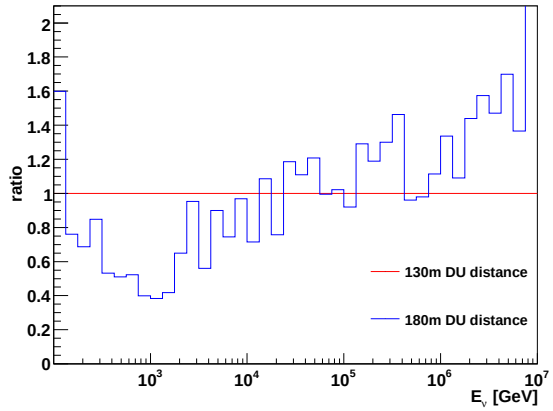

Figure 29: ratio of effective areas

Since the background rates from ^{40}K decays is considered not to vary much and detailed measurements for the different proposed sites were not available, this analysis is a largly theoretical one and can be neglected when evaluating the design options. This simulation also assumes an angular distribution of generated neutrinos of 4π. Only nemo water was used, results are for both zmod and aart reconstruction strategies. The results show a decrease in effective area when background is applied in the simulation. This decrease is roughly constant for the different rates at around 15%, however due to bad statistics (only one file each) it is difficult to quantify the effect. One obvious effect is the massive decrease in effective area for energies below $10^4 GeV$ in case of the aart reconstruction strategy while for zmod only for the lowest energy bins and the highest background rate a similar drop can be observed. It can therefore be concluded that the Aart strategy is far more sensitive to background at low energies than the zmod modification. For energies above 100 TeV both strategies perform similarly and nearly independent from the actual rate of background.

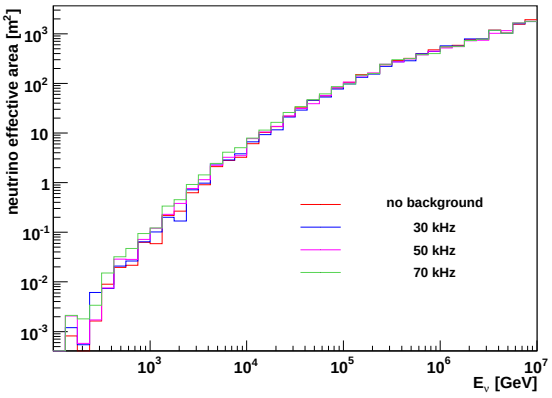

Figure 30: comparison of effective areas, zmod reco algorithm

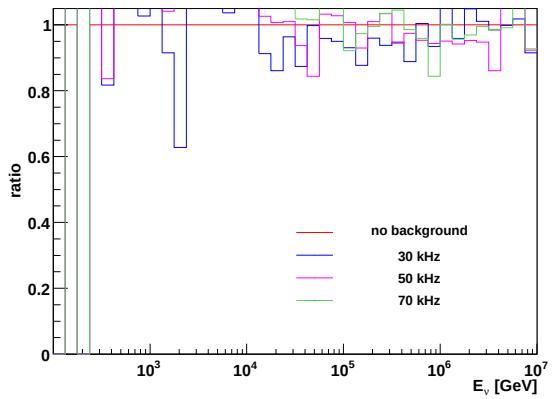

Figure 31: ratio of effective areas, zmod reco algorithm

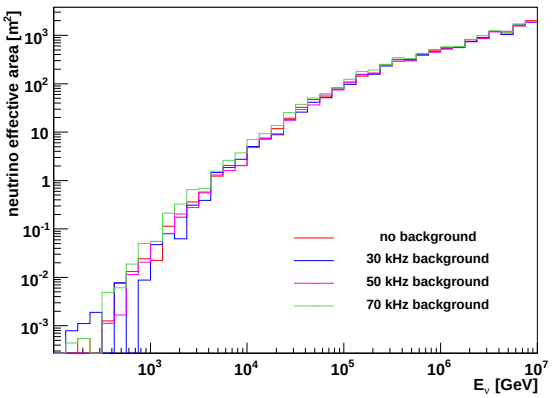

Figure 32: comparison of effective areas, aart reco algorithm

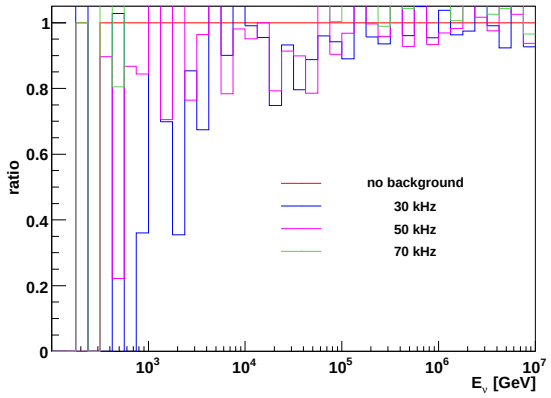

Figure 33: ratio of effective areas, aart reco algorithm

As the reconstruction efficiency is directly affected by the chosen reco strategy the importance of the analysis of their effect on the detector performance can hardly be overestimated. The two available option are the original Aart Strategy and the modified version called zmod in this work. Their differences are explained above. This simulation was performed for nemo water for both 2π and 4π angular distribution of neutrinos. For low energies the zmod strategy yields a far better effective area than the original Aart Strategy (aart) but this increase levels off after 10 TeV. In case of 2π angular distribution the effective area for zmod is 7 times as high as the one for aart at a few hundred GeV and stays 20% higher up until $10^5 GeV$. After that the effective areas are the same for both strategies. For the 4π angular distribution the results are similar but the effective area for both converge already at 20 TeV instaed of 100 TeV for the 2π case. The spike at 1 TeV is considered an artefact and therefore neglected.

The increase in effective area for lower energies in the case of zmod can be explained be the lower limits for number and amplitude of hits compared to aart. Events that would be rejected in aart can thus still be reconstructed in zmod. For higher energies there

are always enough hits with high enough amplitudes to allow reconstruction and so the increase vanishes.

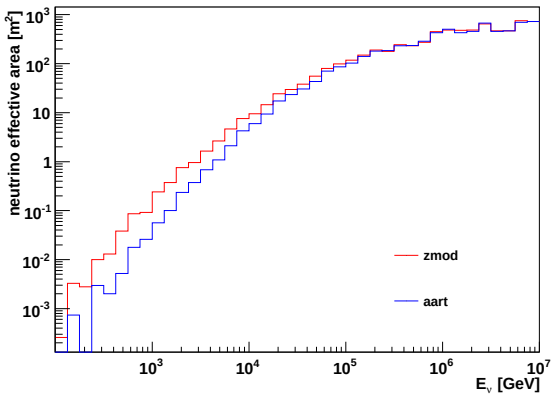

Figure 34: comparison of effective areas, 2π angular distribution

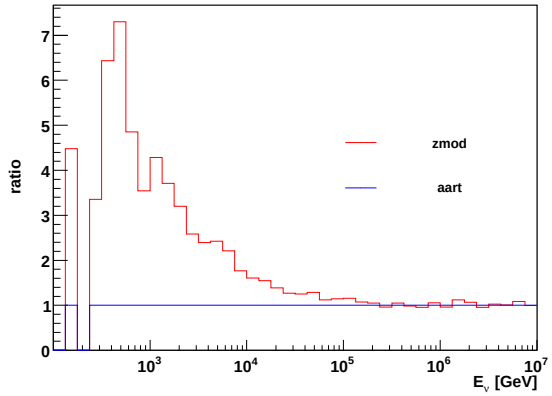

Figure 35: ratio of effective areas, 2π angular distribution

Late in the Design Study it was proposed to increase the number of detection units for the NuONE design to 154 according to supposedly available cost reductions for the DUs. This change is not included in the Technical Design Report and is not considered official but was simulated nontheless before the decision to omit it was final. Since a simulation for a 154-string SeaWiet detector was produced for different reasons this expanded NuONE detector offers an oppotunity for a direct comparison. The increase in surface area of the detector is 5% with going from 127 to 154 detection units. Effective area is higher for the 154 DUs across the whole energy range (neglecting statistical variation) with a tendency for a larger increase at low energies. This increase is on average of the same size as the

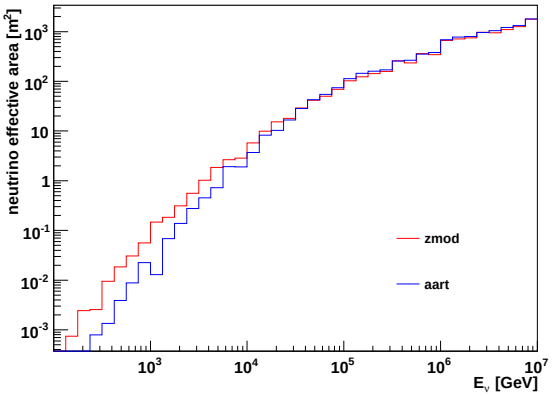

Figure 36: comparison of effective areas, 4π angular distribution

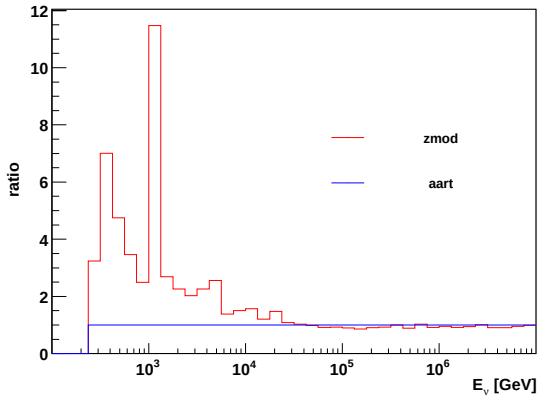

Figure 37: ratio of effective areas,4π angular distribution

increase in surface area although low statistics make a precise measurement difficult. The peak in the first energy bin, especially pronounced in the ratio plot was neglected for the same reason. Simulations performed with aart instead of zmod show the same behaviour, results are only available for angular distribution of 2π.

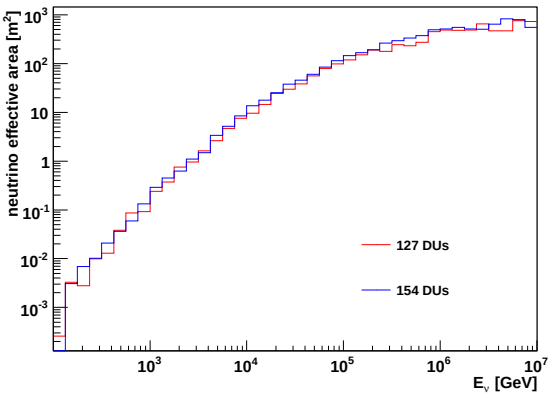

Figure 38: comparison of effective areas

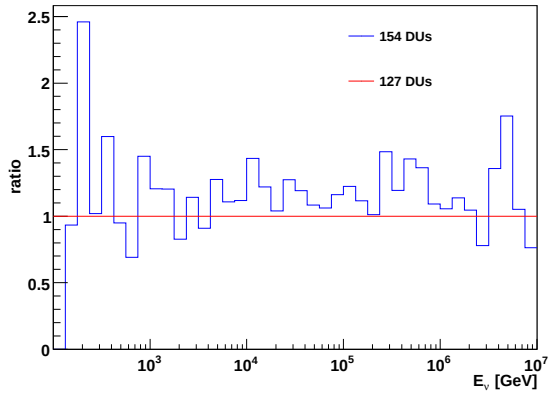

Figure 39: ratio of effective areas

6.2.2 Reconstruction Efficiency

As seen in the description of the neutrino effective area the reconstruction is of crucial importance to detector performance. In this section the reconstruction efficiency will be studied in more detail with regard to the different detector design variations. First it has to be defined what is meant by reconstruction efficiency. Reconstruction efficiency in this study is defined as the number of events that can be reconstructed (number of events after reco) divided by the number of events that cause a detector response (number of events after km3). The number of generated events (number of events from genhen) is higher than those that cause hits. For NuONE the fraction of km3 events (hits) to genhen events (generated events) depends on the angular distribution of the generated neutrinos. In case of 4π distribution the ratio is 51%, for 2π it is 54%. This can be explained by considering that the NuONE optical module is more sensitive to up-going (2π) neutrinos due to the downward looking PMTs. It is harder for down-going neutrinos to cause hits and therefore the fraction is smaller. Also the lower sensitivity to down-going muons means a smaller effect of atmospheric muons which will be described later. The highest overall reconstruction efficiency is achieved for the most densly instrumented detector with the shortest distances between storeys. Another albeit smaller influence is the choice of reco algorithm with zmod performing better than aart, although this difference increases when looking only at up-going neutrinos. The effect of ^{40}K-background is negligible. For shorter absorption lengths the reduction of reconstruction efficiency is also only very small. Besides the overall reconstruction efficiency the different design configurations were evaluated and compared, showing the reconstruction efficiency for the corresponding neutrino energies. The first four plots show the effect of a increase in photocathode area on the reconstruction efficiency by comparing the NuONE storey design with 8-inch PMTs to that with 10-inch PMTs (56% increase in photocathode area). For both reconstruction strategies, aart and zmod, the 10-inch PMT design performs better as can be expected. The increase in efficiency is 5 - 10% up to $10^6 GeV$. At higher energies both PMTs perform similarly, any measurable gain for the larger PMTs is obscured by statistical variation. Note that this comparison uses data with an angular distribution of 4π. The comparison between the designs, NuONE and SeaWiet, uses 2π, therefore those values are slightly different.

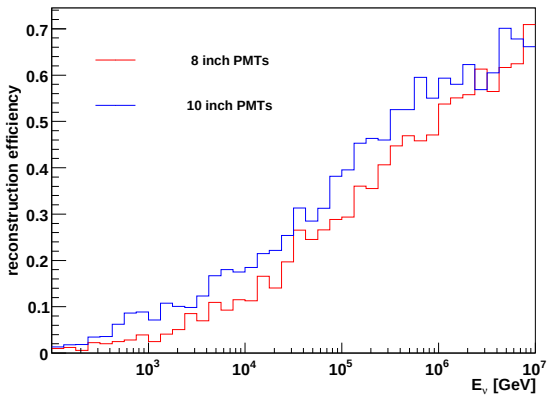

Figure 40: comparison of reconstruction efficiencies, zmod reco algorithm

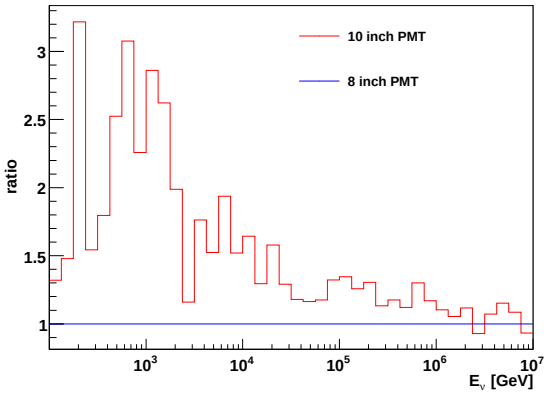

Figure 41: ratio of reconstruction efficiencies, zmod reco algorithm

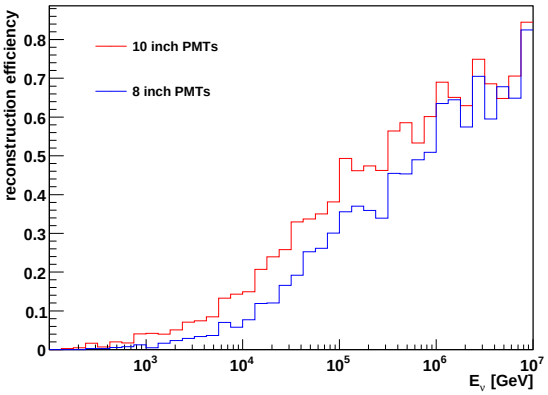

Figure 42: comparison of reconstruction efficiencies, aart reco algorithm

Now the distance between detection units was changed from 180m to 130m. The reconstruction efficiency increases across the whole energy range with a peak of 350% at 1 TeV. Above that energy the increase drop to 200% for energies up to 10 TeV and stays above 20% up until $10^6 GeV$. Only in the last energy decade drops the efficiency for 130m DU distance to the level of 180m DU distance.

In the next simulation the effect of the angular distribution of the generated neutrinos and of the reconstruction algorithm on the reconstruction efficiency was examined. For both angular distributions, 2π and 4π, the same detector was used and both were tested with aart and zmod. In the case of 4π angular distribution the zmod strategy performs on average 5% better than aart in terms of reconstruction efficiency for energies up to 10

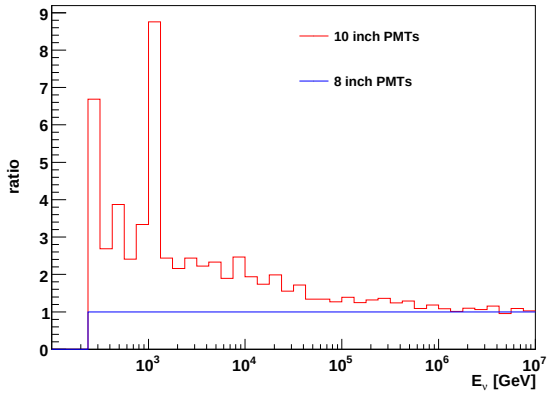

Figure 43: ratio of reconstruction efficiencies, aart reco algorithm

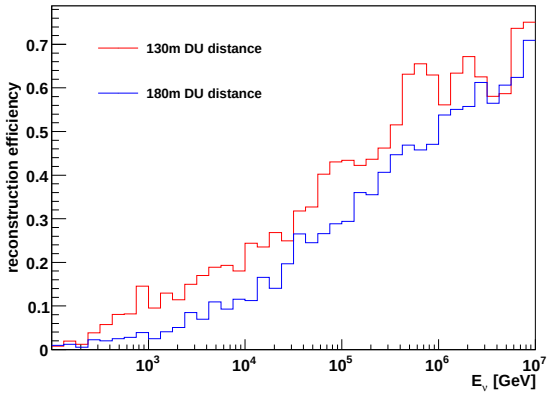

Figure 44: comparison of reconstruction efficiencies, zmod reco algorithm

TeV. Above this threshold both strategies yield roughly the same results with a maximum efficiency of 70% at $10^7 GeV$.

When using an angular distribution of 2π the picture changes. Here, the zmod strategy yields an increase of as much as 10% over aart for energies below 100 TeV. Beyond this energy both strategies produce the same results with larger statistical variations in the last energy decade and an average maximum reconstruction efficiency of 60%.

The difference for the maximum efficiency can be explained by low statistics as is obvious by the large variations in the 2π simulation. This can be shown more clearly when comparing the recostruction efficiencies for both angular distributions. For an angular distribution of 2π the efficiency is 5 - 10% higher than for 4π for energies up to 300 TeV. At higher energies both reconstruction efficiencies are very close to each other execpt for

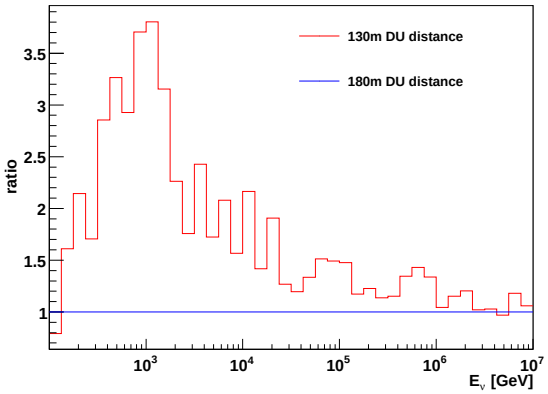

Figure 45: ratio of reconstruction efficiencies, zmod reco algorithm

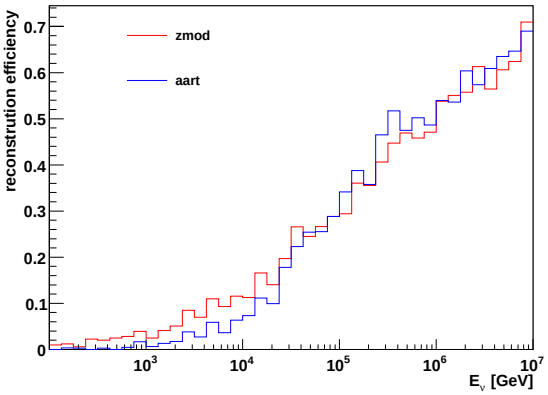

Figure 46: comparison of reconstruction efficiencies, 4π angular distribution

the aforementioned statistical variations in the 2π efficiency. This higher efficiency for up-going neutrinos can already be seen in the ratio of neutrinos causing hits (km3) and generated neutrinos (genhen), which is higher for up-going only neutrinos.

Another property that affects the reconstruction efficiency is the ^{40}K background rate. Since the simulation used identical detector designs the only factor that changed the effective area is the reconstruction efficiency. For a more detailed view see the chapter on effect of ^{40}K background on effective area.

To evaluate to influence of the absorption length on the efficiency, a comparison of the two water models nemo and asbw has been made using the zmod reco algorith and a 4π angular distribution of generated neutrinos. The ratio of the efficiencies follows closely the ratio of the corresponding effective areas (see above), albeit on a smaller scale since the larger can size for nemo water is not accounted for in this simulation.

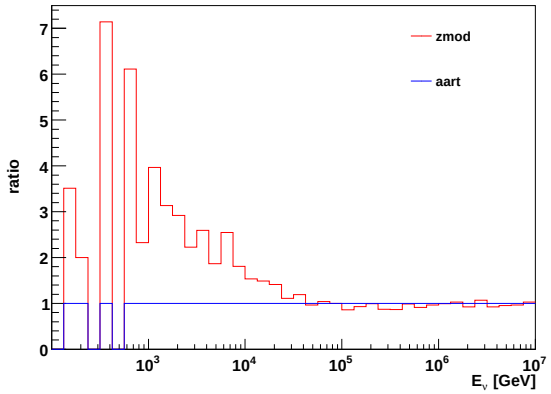

Figure 47: ratio of reconstruction efficiencies, 4π angular distribution

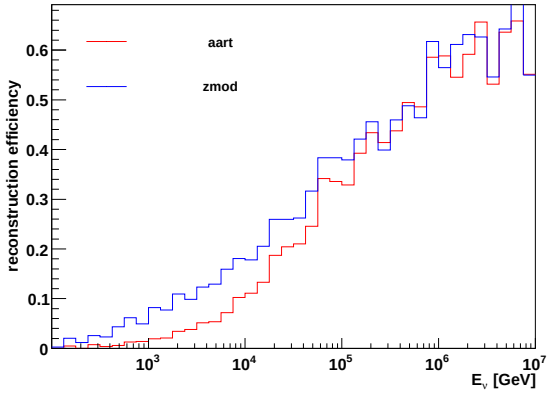

Figure 48: comparison of reconstruction efficiencies, 2π angular distribution

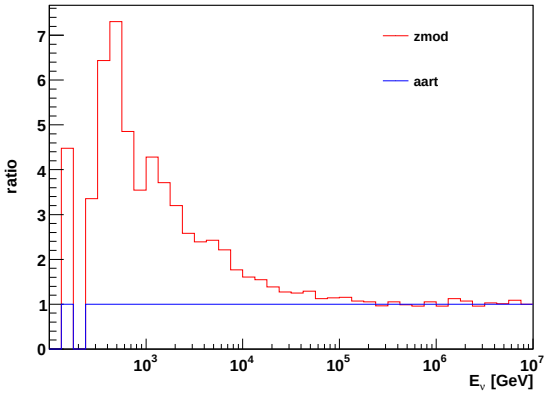

Figure 49: ratio of reconstruction efficiencies, 2π angular distribution

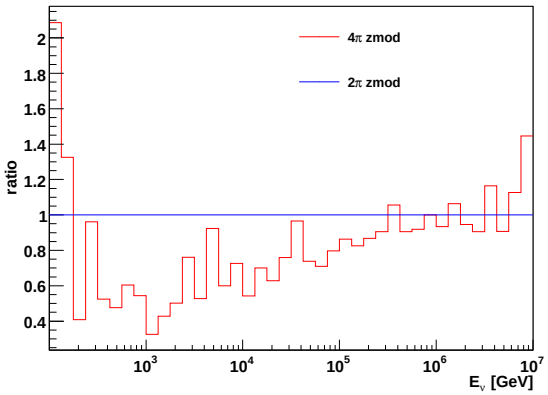

Figure 50: ratio of reconstruction efficiencies, zmod reco algorithm

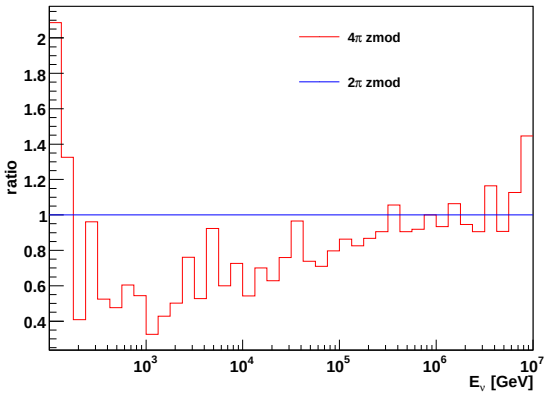

Figure 51: ratio of reconstruction efficiencies, zmod reco algorithm

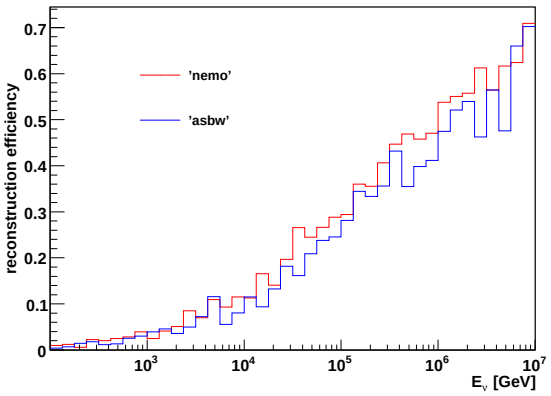

Figure 52: comparison of reconstruction efficiencies, zmod reco algorithm

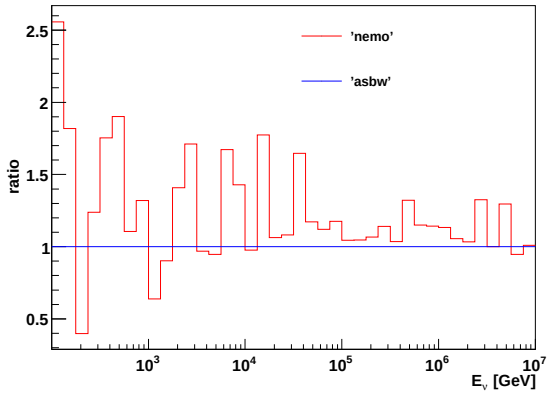

Figure 53: ratio of reconstruction efficiencies, zmod reco algorithm

6.2.3 Atmospheric Muon Background

The simulation of the atmospheric muon background was performed only up to the km3 level, i.e. only the detector response was simulated, no reconstruction was attempted. Also the study is limited to only one depth (3500m) and one water type (nemo) using the NuONE 127 detection unit layout with a DU distance of 180m. Both the 8-inch and the 10-inch PMTs were used with 5×10^6 muons simulated for each configuration. This corresponds to a total livetime of 1380s in both cases. For the 8-inch PMTs 25% of all generated muons cause a detector response. The background rate from atmospheric muons in this configuration is 904Hz. In case of the 10-inch PMT storey configuration 29% of the atmospheric muons result in a detector response. This amounts to a background rate of 1040Hz. The 56% increase in photocathode area, from $324.3cm^2$ to $506.7cm^2$ yields only a 15% higher background rate.

6.3 Summary for NuONE

To better show the results for the effective area, averages were used where more than one file was available. Also the effective areas were calculated for both neutrinos and anti-neutrinos as well as an average effective area, assuming a ratio of neutrinos and antineutrinos of 1 : 1. The different effective areas for neutrinos and anti-neutrinos are caused by the different neutrino-nucleon cross section $\sigma(E_\nu)$ for these particles. A comparison between the reconstruction efficiencies of neutrinos and anti-neutrinos shows only very minor differences with the efficiency for anti-neutrinos a little lower than that for neutrinos 5% on average for $E_\nu > 10TeV$.

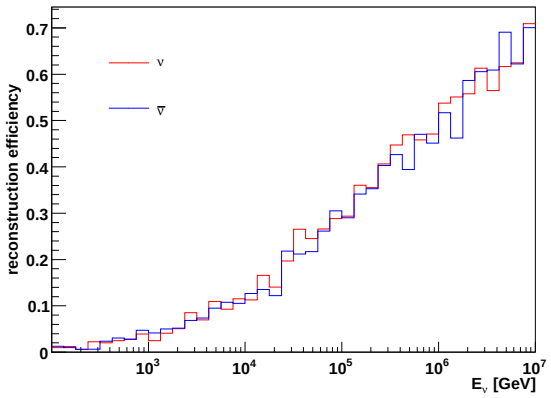

Figure 54: comparison of reconstruction efficiencies, zmod reco algorithm

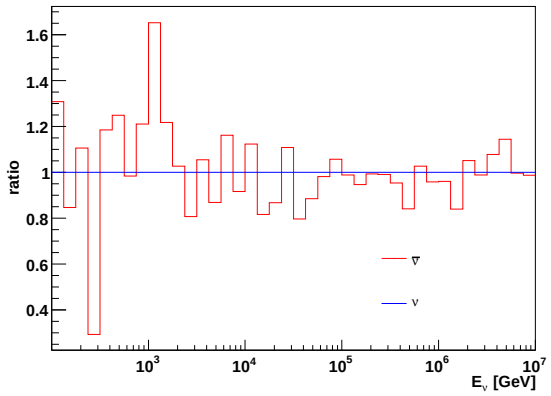

Figure 55: ratio of reconstruction efficiencies, zmod reco algorithm

The analysis of the effects of the various simulation parameters, both environmental and design parameters, can even where statistics were low give a general trend with regards

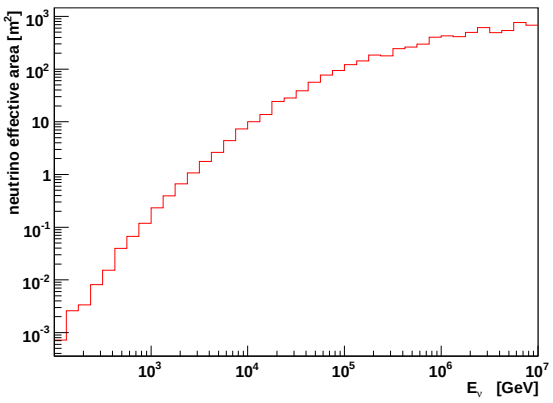

Figure 56: average effective area, zmod reco algorithm, 2π angular distribution

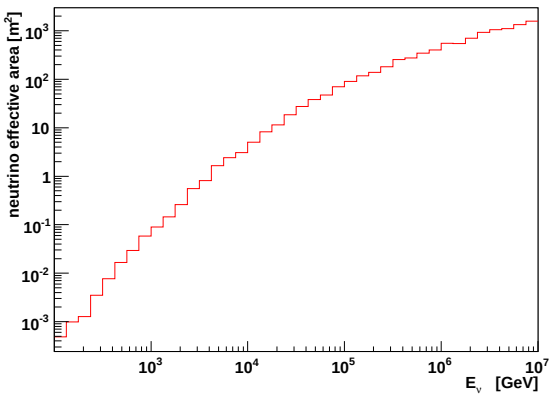

Figure 57: average effective area for neutrino and anti-neitrinos, zmod reco algorithm, 4π angular distribution

to the optimisation of these parameters. The most obvious way to optimise the detector performance is to select a site which has water with a high absorption length. The increase in absorption length causes a nearly as big an increase in effective area. Another way to get a higher effective area is by increasing the number of detection units, which results in an increase in performance congruent with the increase in photocathode area. Switching from 8 inch to 10-inch PMTs will also increase the effective area, although not on the same scale as the increase in photocathode area, only around 30% for high energies rather than the 56% gain in photocathode area. To evaluate the effect of the instrumentation density it is necessary to look closer at the neutrino energy spectrum. For energies lower than 10 TeV the increase in density and the corresponding increase in effective area outweighs the decrease caused by the reduced detector volume. At energies above 10 TeV the density of the instrumentation becomes less relevant and the increse in detector volume becomes the dominating effect on the effective area. To make a meaningful statement as to the optimal density (DU distance) of the detector it would therefore be necessary to determine which part of the neutrino energy spectrum is to be investigated. For high energies the most relevant parameter is the detector volume. The choice of reco algorithm is also less

important at these high energies ($> 10^6 GeV$), while for lower energies the zmod strategy is preferable to achieve high effective areas. It needs to be cautioned though, that this study does not include a detailed analysis of the quality of these reco algorithms, for example mean angular error and energy reconstruction.

6.4 Results for SeaWiet

In the study of the SeaWiet design option seven parameters were varied to evaluate their effect on the performance of the detector. The photocathode was left the same at 3 inch diameter, the number of storeys per string at 20.

6.4.1 Effective Area

For the analysis of the SeaWiet detector the same variation of the angular distribution of the neutrinos was used as for the NuONE design with 2π designating the up-going neutrinos. The detector configuration for the simulation is the SeaWiet version with 310 strings in hexagonal layout and 40 metres storey distance. The effective area for 2π angular distribution is higher for energies below $10^5 GeV$, compared to 4π as much as 40% for the first energy bins. Above $10^5 GeV$ the effective area drops compared to 4π to only half the value in the last energy bins. The simulation was done with nemo water and the zmod reconstruction strategy.

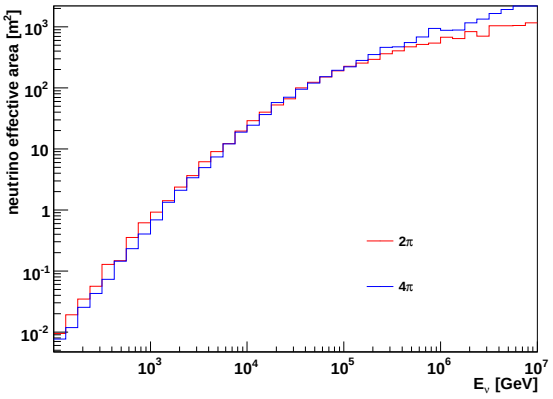

Figure 58: comparison of effective areas, zmod reco algorithm

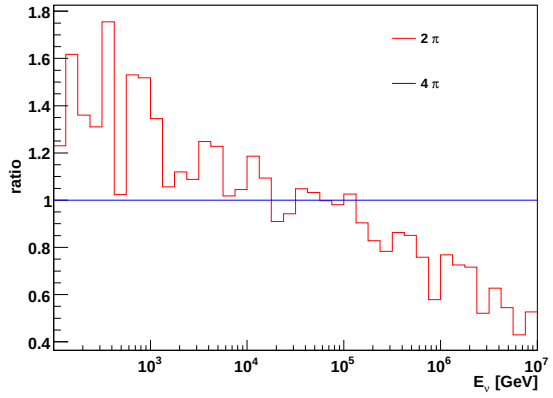

Figure 59: ratio of effective areas, zmod reco algorithm

As with the NuONE study the two water models asbw and nemo were used, the nemo this time with two different scatter models. This simulation was performed for the 300 string octogonal layout configuration using both the aart and zmod strategies. For the

effective area an increase of on average 20% across the energy range is observable for the change from asbw to nemo water models. This increase is approximately the same for both reconstruction strategies and is a little higher for low energies than for higher ones. Due to low statistics more precise estimates are not possible.

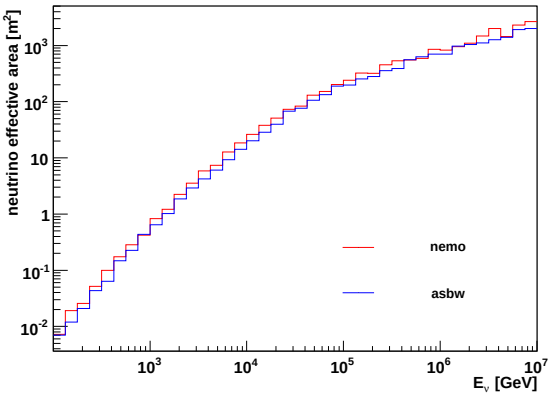

Figure 60: comparison of effective areas, zmod reco algorithm

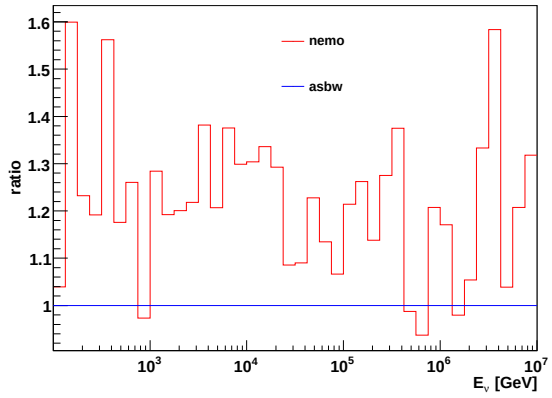

Figure 61: ratio of effective areas, zmod reco algorithm

The effect of different scattering lengths is far less than that of different absorption lengths. For an increase of scattering length by a factor of 4.5 the gain in effective area is only 15%. This simulation was performed for the 310 string hexagonal design with 40m storey distance using the zmod strategy and up-going neutrinos only (2π angular distribution). The higher effective area for longer scattering length is due to less scattering resulting in a higher density of the photon field, allowing for more hits on the PMTs within the defined time window to be counted as one single hit. With more photons per such hit

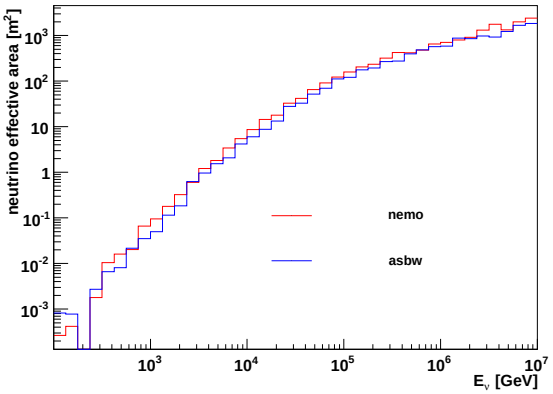

Figure 62: comparison of effective areas, aart reco algorithm

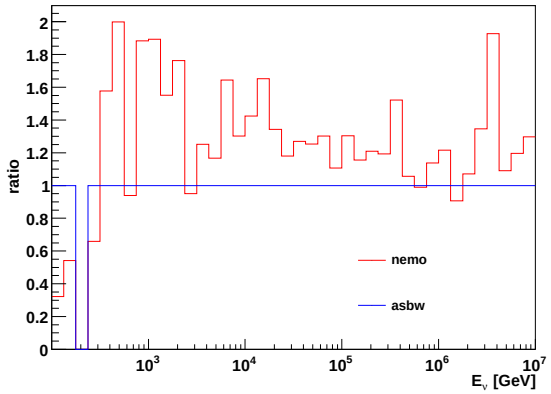

Figure 63: ratio of effective areas, aart reco algorithm

the amplitude increases resulting in more hit events with an amplitude above the defined threshold. So more hits can be reconstructed increasing the reconstruction efficiency.

The study for the different detection unit distances was performed for the design option with 300 strings in an octogonal layout. Again the the effects of variable instrumentation densities and volumes on the effective area are analysed. The effective areas were calculated for 90m, 130m and 150m DU distance. Below $4 \times 10^4 GeV$ the 90m configuration performs best with an effective area 20% - 30% higher than the larger detectors. Beyond 10 TeV the larger detectors have higher effective areas, the volume effect surpasses the better reconstruction efficiency for the small detector. The effective area for the larger DU distances rises to two times the value of the 90m DU distance configuration in the energy range above $10^6 GeV$. Both the 130m and the 150m configuration perform very similarly with the 150m one 5% - 10% better than the 130m detector. The big differences in the high energy ($> 10^6 GeV$) range are caused by low statistics.

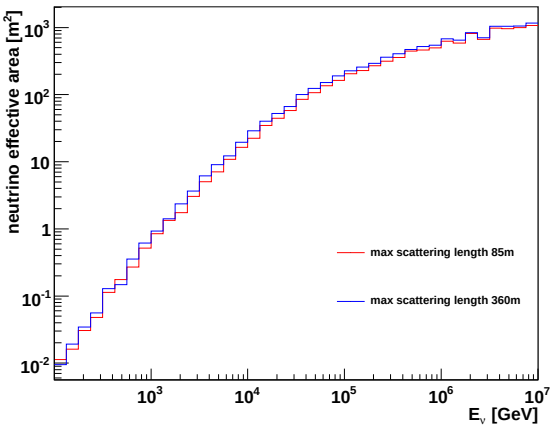

Figure 64: comparison of effective areas, zmod reco algorithm, 2π angular distribution

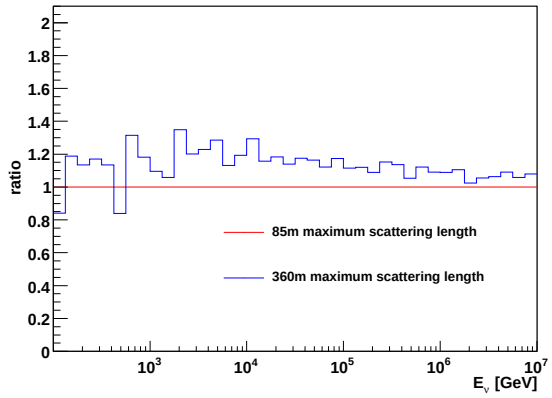

Figure 65: ratio of effective areas, zmod reco algorithm, 2π angular distribution

A comparable result is achieved by the comparison of two different detection unit distances for the 310 string hexagonal layout. Here the effective areas for 130m and 150m are shown. Again the larger detector becomes better in terms of effective area at 10 TeV and yields an on average 10% higher effective area for higher energies with low statistics obfuscating a clearer result. Note that the absolute values are lower for this comparison since only an angular distribution of 2π was used compared to 4π for the octogonal layout.

The same considerations for the study of the effect of background on the effective area apply as in the case of the NuONE design. For the octogonal 300 string design 2, 4, 6 and 8 kHz ^{40}K background was simulated. The differences in effective area are only due to different reconstruction efficiencies since the detector volume remains unchanged. The reconstruction efficiency decreases with increasing background rate in the TeV energy range although the differences are small and not always consistent. For lower energies rates of 6kHz and 8kHz result in higher effective areas due to misreconstructed hits that

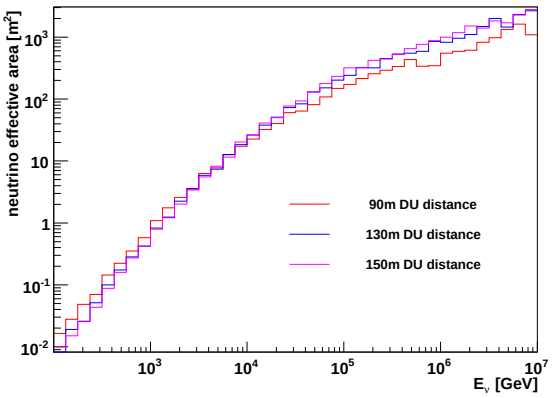

Figure 66: comparison of effective areas, zmod reco algorithm, 4π

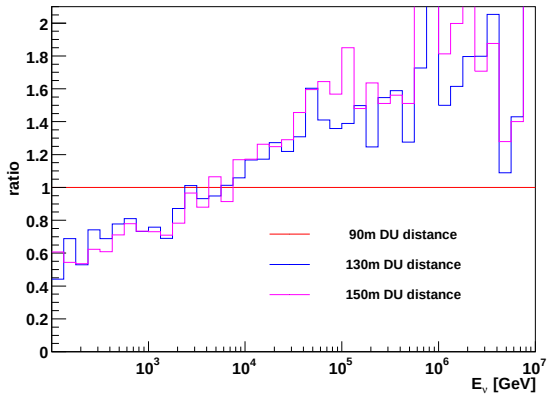

Figure 67: ratio of effective areas, zmod reco algorithm, 4π

are actually background events. Beyond $10^6 GeV$ the effect of background diminishes since background events can no longer influence the amplitude of hits, there are enough hits with high enough amplitudes to allow for correct reconstruction. For lower energies the presence of background induced hits can allow events to be reconstructed which proper hits are by itself too few in number or have a too low amplitude to avoid being rejected by the reco algorithm. Because these events would not be detectable if it were not for the background, these are considered misreconstructed. The used software does not account for background events mimicking true events. The drop in effective area is as much as 20% for 8 kHz background rate around 5 TeV. For the hexagonal 310 string layout the effects are even more visible. Here the drop reaches 30% for the 8 kHz background rate around 5 TeV. Why the reconstruction efficiency for 4 kHz is worse than for 8 kHz is unknown. The effect of background are also noticeable for a wider energy range becoming neglectible only above $8 \times 10^7 GeV$. Since the parameters for the two layouts are the same and the same detection unit is used, the differences are an effect of statistical variation.

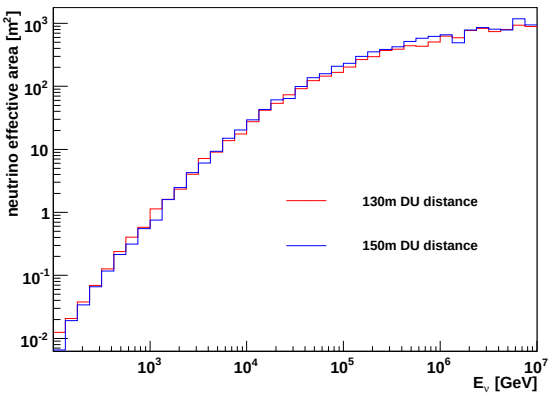

Figure 68: comparison of effective areas, zmod reco algorithm, 2π

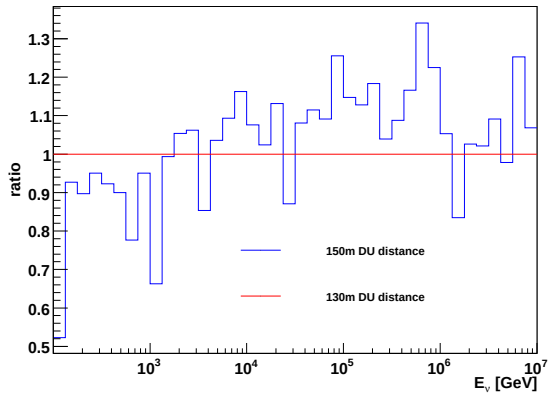

Figure 69: ratio of effective areas, zmod reco algorithm, 2π

For the aart strategy the picture is worse. Here the effective area is massively reduced at lower energies with a drop of 65% at 5 TeV for 4kHz and 8 kHz background rate. The results for both 4 kHz and 8 kHz are very similar, the reason for the inconsistent results for the 6 kHz is unknown. Again the decrease diminishes above $10^6 GeV$. The baseline for all SeaWiet simulations studying background are the results for a background rate of 2 kHz.

As described in the description of SeaWiet the first design option consisted of 300 strings in an octogonal layout. This was later changed into a hexagonal layout with 310 strings. Here the effect of the design change is analysed. Up to 10 TeV the hexagonal detector performs better due to the denser instrumentation. There are six neighbouring lines within 130m for the hexagonal, four neighbouring lines within 130m for the octogonal layout. Additionally, the photocathode area is 3% larger for the 310 string design. Above 10 TeV the larger volume for the octogonal design dominates over the improved reconstruction efficiency of the hexagonal layout caused by the denser instrumentation. Beyond $10^6 GeV$ the effective area for the 300 string octogonal detector is on average 10% higher than that of the 310 string hexagonal one. This simulation assumed 4π angular distribution of

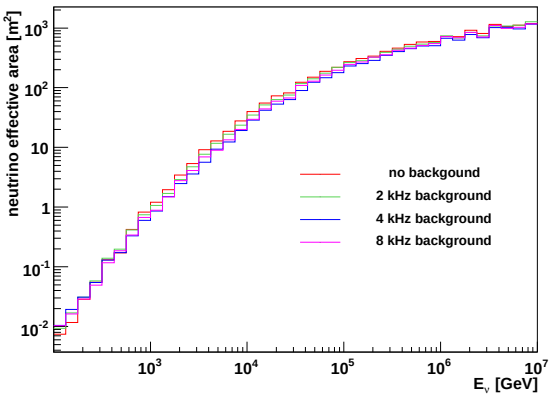

Figure 70: comparison of effective areas, zmod reco algorithm, 2π

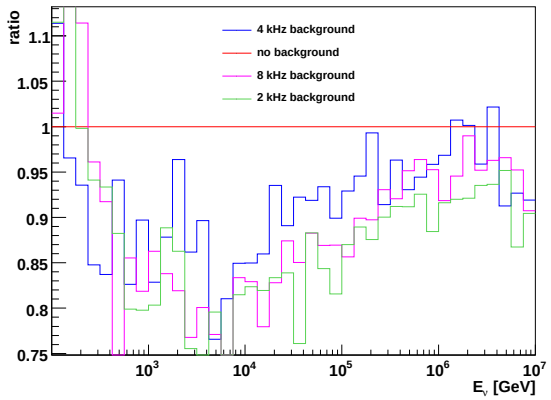

Figure 71: ratio of effective areas, zmod reco algorithm, 2π

generated neutrinos and used the zmod reco strategy.

Late during the Design Study an increase in storey distance was proposed. The distance was changed from 30m to 40m in this study resulting in a larger, less densly instrumented volume. The increase in instrumented volume is 25%. Below 10 TeV the more densely instrumented detector perform better by an average of about 10%, for energies higher than several tens of TeV the larger detector with its larger volume can outperform the more efficient smaller but denser detector, exceeding the effective area by 20% for the highest energies. This simulation was done for the 310 string hexagonal detector using zmod and 2π angular distribution.

Again the effects of the two different reco strategies aart and zmod are analysed. In case of the multi-PMT storey of the SeaWiet design it has to be emphasised that both

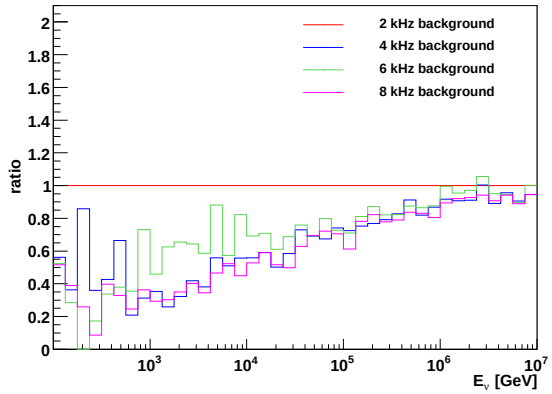

Figure 72: ratio of effective areas, aart reco algorithm

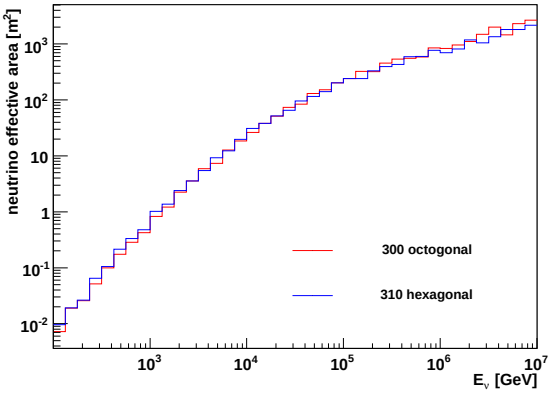

Figure 73: comparison of effective areas, zmod reco algorithm

of these strategies were created with the ANTARES storey or something very similar in mind. Therefore the application of the strategies to the multi-PMT design is not without potential pitfalls. A reconstruction strategy specifically designed for SeaWiet will eventually become necessary to avoid these possibly problems. For the moment there are no PDFs for this design. The aart reco strategy performs poor compared to zmod across the whole energy range. Especially for energies below 10 TeV where the effective area for aart stays below 30% for that of zmod. For higher energies aart fares better, reaching 50% at 40 TeV and 60% just above 100 TeV. Above $10^6 GeV$ the effective area reaches a maximum of 80% of the value for zmod. This simulation was performed for the 310 string hexagonal design with 40m storey distance and an angular distribution of 2π.

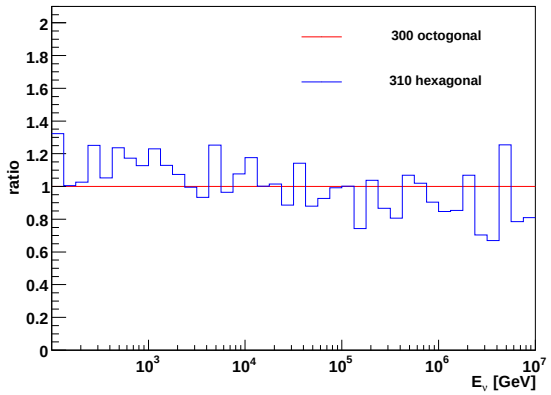

Figure 74: ratio of effective areas, zmod reco algorithm

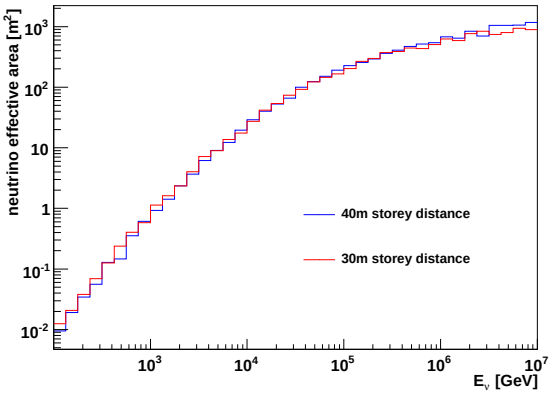

Figure 75: comparison of effective areas, zmod reco algorithm

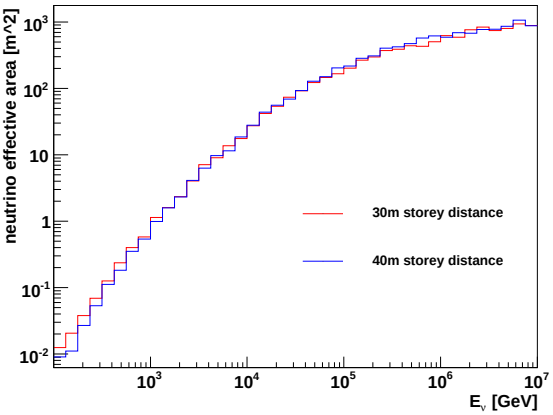

Figure 76: ratio of effective areas, zmod reco algorithm

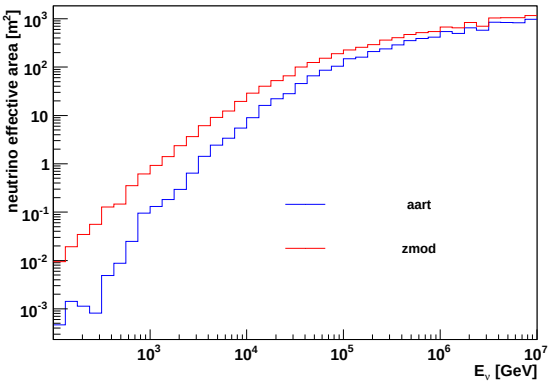

Figure 77: comparison of effective areas, 2π

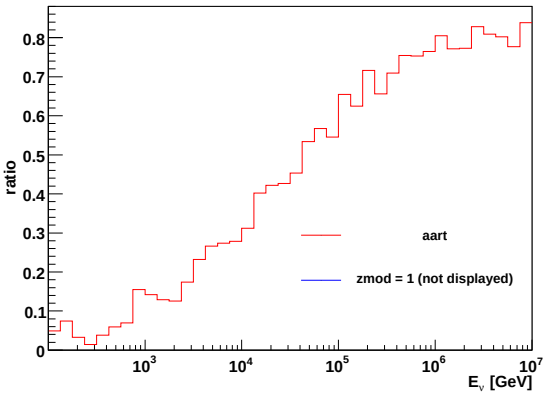

Figure 78: ratio of effective areas, 2π

6.4.2 Reconstruction Efficiency

Aside from the above mentioned issues there seems to be no obvious flaw in the reconstruction. So again the reconstruction efficiency will receive a more detailed treatment. The reconstruction efficiency used for SeaWiet is the same as for NuONE. Again the number of genhen events is higher than the number of km3 events. However, in case os the SeaWiet design the fraction of events actually causing hits in the detector is independent from the angular distribution of the generated neutrinos. This is due to the design of the optical module which is not only equiped with downward-facing PMTs like the NuONE OM but also features upward-looking PMTs. The bias towards up-going neutrinos is therefore eliminated. In both the 2π and the 4π angular distribution cases the ratio of detected events to incoming events is 55%, close to the 54% for up-going neutrinos in NuONE detectors. The effect of down-going atmospheric muons will be examined in the next part of this study. The following part is an in-depth look at the reconstruction efficiency for the different configurations with respect to the neutrino energy. The angular distribution of the generated neutrinos was varied between 4π and 2π (up-going). This simulation was only performed for one configuration, the 310 string hexagonal layout with 40m storey distance and the zmod reco algorithm. Below 10 TeV the efficiency is higher for the 2π angular distribution, above the value for the 4π distribution is higher. Since one cannot simply turn off neutrinos coming from above or below, these results are more important when comparing different simulations than evaluation one specific design.

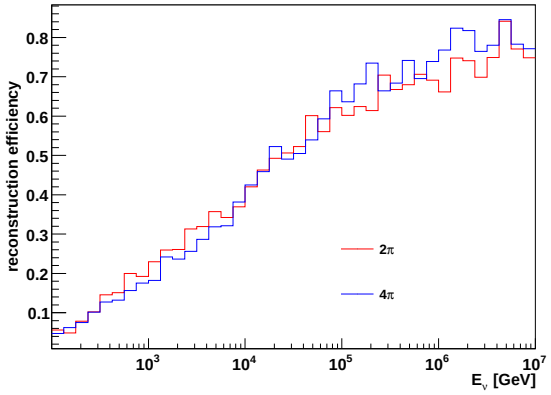

Figure 79: comparison of reconstruction efficiencies, zmod reco algorithm

The study of the different water model includes are variant of nemo with different scattering lengths, called 0075. For the comparison between asbw and nemo the 300 string octogonal layout was chosen. The simulation show no consistent difference in the reconstruction efficiency for the two different absoprtion models.

To determine how the scattering length influences the reconstruction efficiency, two different scattering models were implemented in the simulation. This was done only for

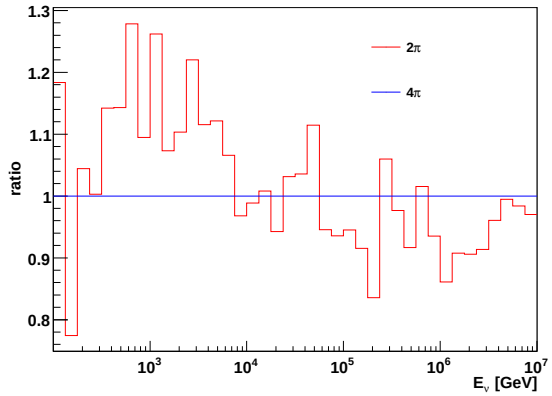

Figure 80: ratio of reconstruction efficiencies, zmod reco algorithm

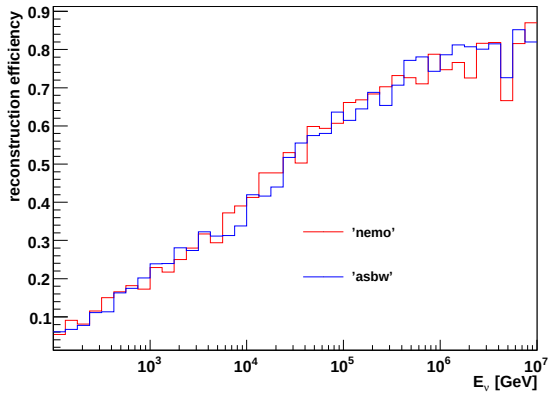

Figure 81: comparison of reconstruction efficiencies, zmod reco algorithm

the 310 string hexagonal design with a distance between storeys of 40m. The efficiency is on average 10% lower for the 0075 scattering model with maximum scattering length of 85m than for those with a maximum scattering length of 360m. Shorter scattering length means more scattering takes place which leads to a thinning of the photon field and in turn to lower hit amplitudes.

For the effect of ^{40}K-background on the reconstruction efficiency the comparison was only made for the 310 string design with 40m storey distance and a 2π angular distribution of generated neutrinos. Aside from the fact that a different design was used the results here are the same as in the analysis of the effective area noted above. Since any change in this comparison for the effective area is a different background rate and therefore the reconstruction efficiency, there is no need to repeat the whole exercise for the 300 string octogonal design. Again the effect of the background rate depends on the energy, with the biggest loss, about 15%, between 1 TeV and 10 TeV and on average 5% beyond that energy. The apparent increase in reconstruction efficiency for energies higher than $4 \times 10^6 GeV$ can only be explained by misreconstructed events (see above).

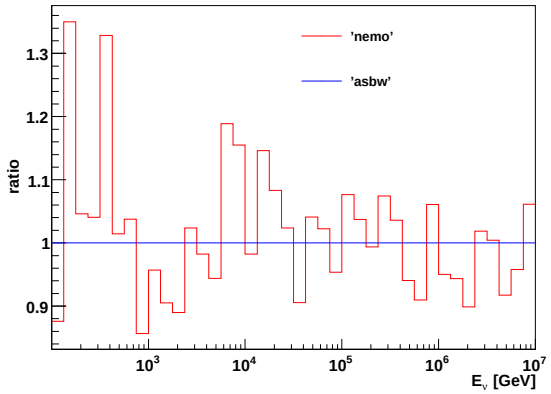

Figure 82: ratio of reconstruction efficiencies, zmod reco algorithm

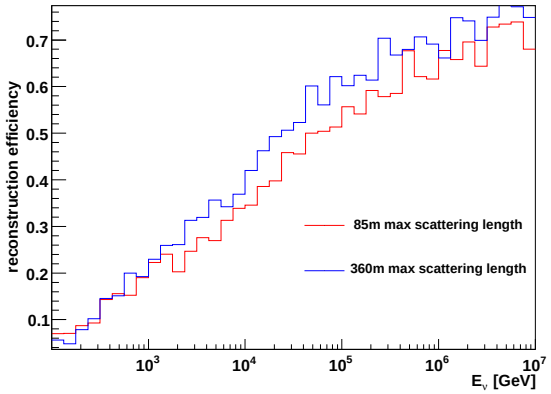

Figure 83: comparison of reconstruction efficiencies, zmod reco algorithm

Towards the end of the Design Study the SeaWiet surface layout was changed from a 300 strings octogonal layout to a 310 strings hexagonal layout. This not only increases the photocathode area available by ca. 3% but also results in a more densly packed detector. The comparison here is between the two geometries with only the zmod strategy used. The hexagonal layout outperforms the octagonal one for energies up to 100 TeV, around 20% for the decades between 100 GeV and 10 TeV. At energies higher than 100 TeV the two geometries perform comparably in terms of reconstruction efficiency, with differences mostly due to low statistics.

Another design parameter is the distance between individual storeys on the detction units. Here the 310 string hexagonal design was simulated with two different storey distances, 30m and 40m. Note that the number of storeys was kept constant, so the instrumented volume is 25% higher for the design option with 40m storey distance which should not affect the reconstruction efficiency. As can be expected from the denser instrumentation, the design with the smaller spacing between storeys performs better.

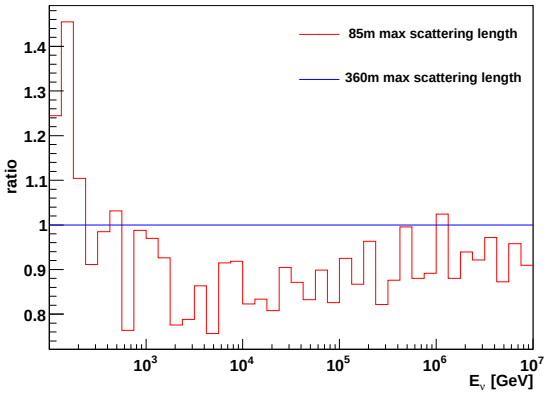

Figure 84: ratio of reconstruction efficiencies, zmod reco algorithm

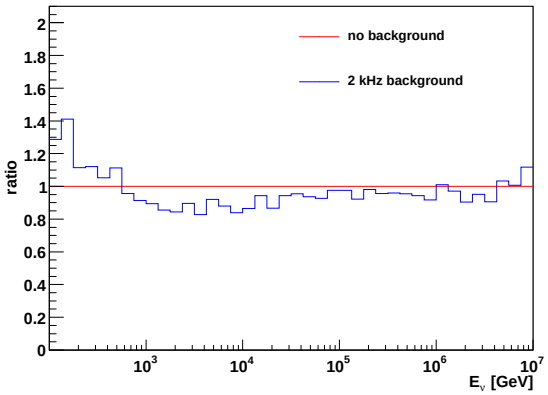

Figure 85: comparison of reconstruction efficiencies, zmod reco algorithm

For low energies the gain in reconstruction efficiency from reducing the storey distance by 25% is more than 50% in the range of 100 GeV - 1 TeV, 20% for up to 10 TeV and 10% for energies up to $4 \times 10^5 GeV$. At higher energies the picture gets disturbed by the lack of statistics but it is reasinable to assume that the reconstruction efficiencies converge beyond $10^6 GeV$ to a maximum of 85% for the last energy decade.

As can be expected, the choice of reconstruction strategy is crucial to the achievable reconstruction efficiency. For the study of the effect of the two reco algorithms, aart and zmod, the 310 string hexagonal design was used (4π angular distributon). The improvement when using zmod instead of aart is massive for the energies below 10 TeV (more than 300%) with a maximum of over 2000% for energies around 350 GeV. For the energy range above 10 TeV it is still 50% for up to 100 TeV, 20% for up to 1 PeV and 10% for energies up to 10 PeV.

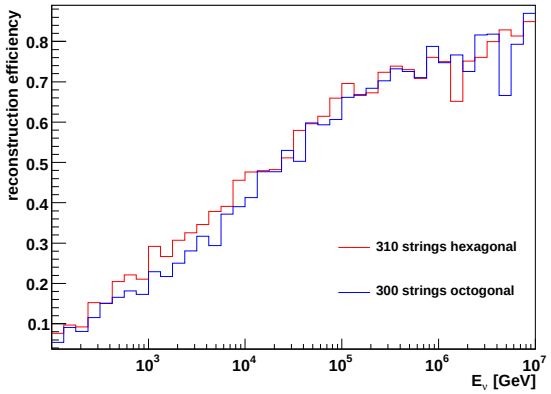

Figure 86: comparison of reconstruction efficiencies, zmod reco algorithm

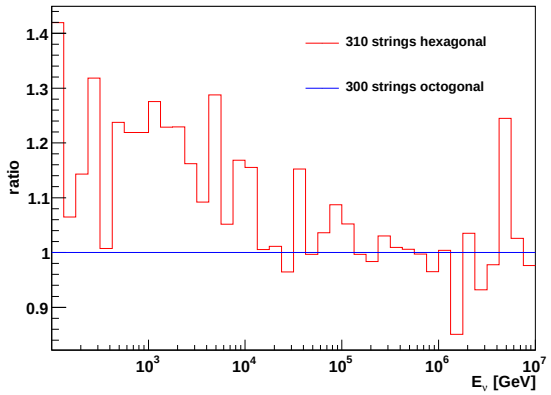

Figure 87: ratio of reconstruction efficiencies, zmod reco algorithm

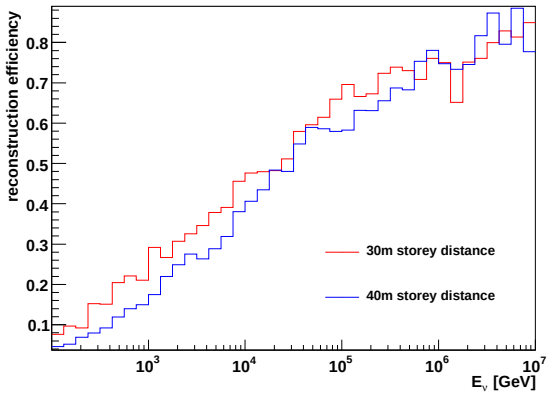

Figure 88: comparison of reconstruction efficiencies, zmod reco algorithm

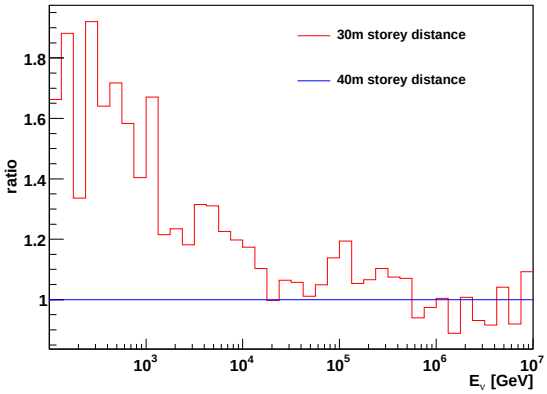

Figure 89: ratio of reconstruction efficiencies, zmod reco algorithm

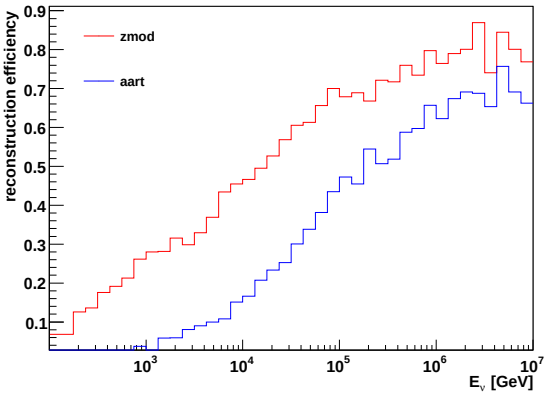

Figure 90: comparison of reconstruction efficiencies

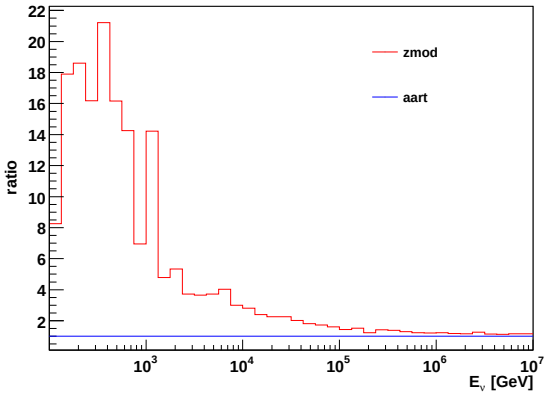

Figure 91: ratio of reconstruction efficiencies

6.4.3 Atmospheric Muon Background

Due to the space and CPU time requirements of the mupage simulations only the latest SeaWiet design with 310 strings in hexagonal layout, 130m DU distance and 40m storey distance. The simulation for atmospheric muons was performed for two depths, 3500m and 4500m. For a depth of 3500m 3×10^5 muons were simulated corresponding to a total livetime of 67.2s. Of those 3×10^5 muons 38.8% cause a detector respone. Reconstruction with the zmod algorithm is possible for 6.1% of those events. Background rate is 1.73kHz At a depth of 4500m the muon flux is lower so the 3×10^5 muons here correspond to a total livetime of 274.5s. The fraction of those resulting in detector response is 39.6%, of these 6.5% can be reconstructed using zmod. The background rate for this depth is 0.43kHz. This means that going from 3500m down to 4500m will decrease the background rate by 75%.

6.5 Summary for SeaWiet

As with the NuONE detector the effective areas for neutrinos and anti-neutrinos are shown separately as well a combined average again assuming a ratio of neutrino to anti-neutrino of 1 : 1. Design configuration is the 310 string detector with storey spacing of 40m.

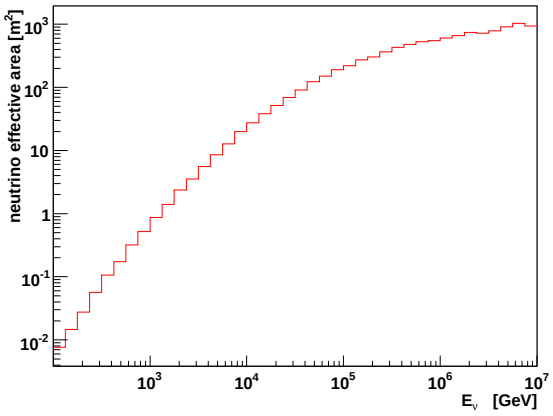

Figure 92: average effective area, zmod reco algorithm, 2π

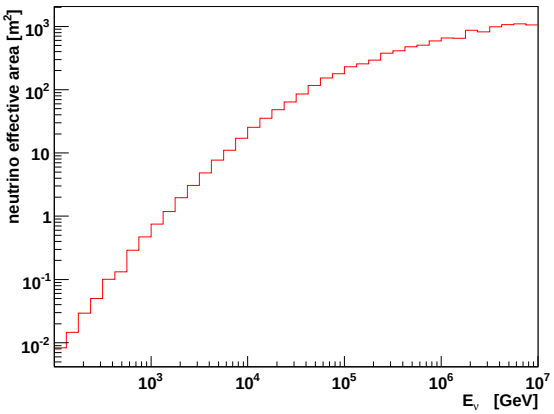

Figure 93: average effective area for mix of ν and $\bar{\nu}$, zmod reco algorithm, 2π

The considerations for the site selection as a measure to optimise detector performance are the same as in the case of NuONE. Again the tipping point is 10 TeV, when the improved reconstruction efficiency due to denser spacing of storeys (DU distance and storey distance) gives way to the increase in instrumented volume. The layout geometry should therfore be chosen as to cover a larger surface area and an increase of 10% in effective area can be gained by increasing the vertical spacing of the storeys by 10m (25%). Since for this

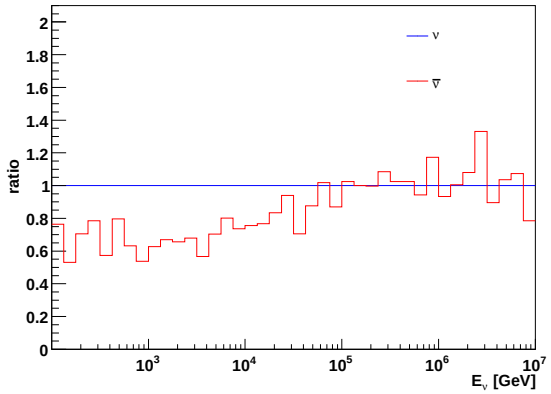

Figure 94: ratio of effective areas, zmod reco algorithm, 2π

design the atmospheric muon background was actually simulated for two depths, it can also be recommended that beyond the water properties, the deepest reasonable site is to be chosen. As was seen, the additional 1000m of water reduce the atmospheric background by 75%. Use of zmod is again recommended although the same cautionary warning as in case of NuONE apply here as well.

7 Double-sized Detectors

In the last phase of the preparation of the Technical Design Report (TDR) it was decided that the WP2 contribution should include an analysis of double-sized detectors. This double-sized detector should be composed of two normal-sized detectors, either design, and to be placed a few kilometres apart at the same site. The reason for this is that calculation of effective areas is easier since no new simulations are necessary, the effective areas for the single-sized detectors can simply be doubled and because the individual can volumes do not overlap, a larger effective area can be achieved for two individual detectors than for a detector with twice as many detection units. To demonstrate this a SeaWiet detctor with 310 strings in hexagonal layout was compared to two 154 string SeaWiet detectors, also with hexagonal layout.

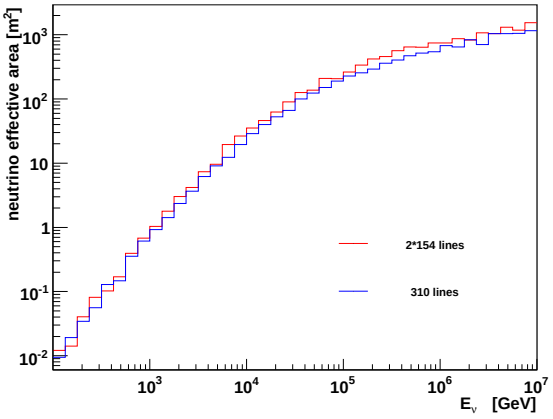

Figure 95: comparison of effective areas, zmod reco algorithm

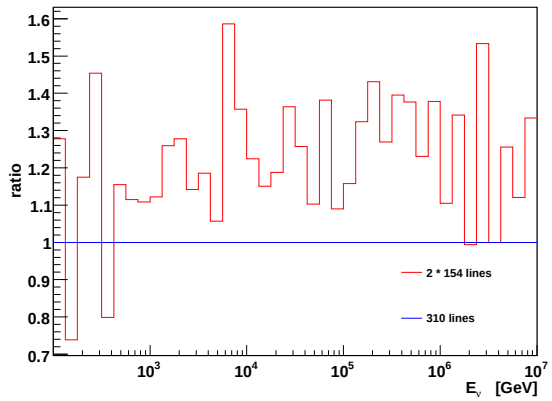

Figure 96: ratio of efective areas, zmod reco algorithm

The same doubling was performed both for the NuONE and the SeaWiet design. All simulations use 2π angular distribution of generated neutrinos. For NuONE, the standard design (127 DUs, 180m DU distance) was chosen, for SeaWiet the 310 string configuration with 40m storey distance.

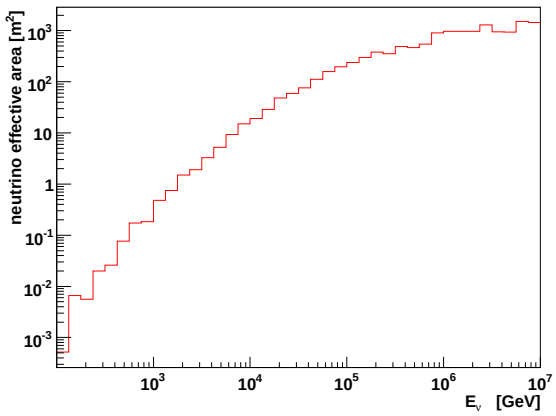

Figure 97: effective area of double-sized NuONE detector, zmod reco algorithm

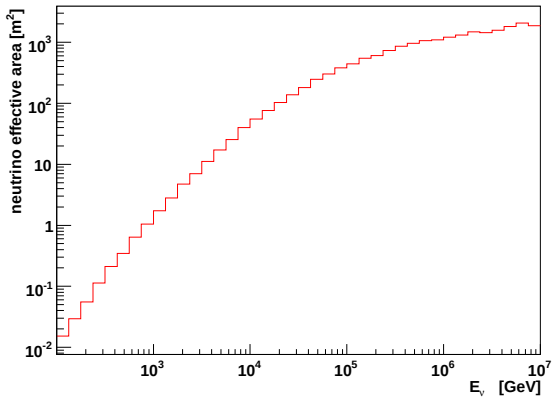

Figure 98: average effective area of double-sized SeaWiet detector, zmod reco algorithm

8 Comparison

For comparison two of each of the two design options were chosen. For the SeaWiet designs the 310 string hexagonal layout with the two different storey distances, 30m and 40m, were used, while for the NuONE design two different photomultiplier sizes, 8 inch and 10 inch, were chosen. The detection unit distance for the SeaWiet design was fixed at 130m and at 180m for the NuONE design. The simulation properties are the nemo water, 2π angular distribution and the zmod reconstruction algorithm. Both the effective areas and the reconstruction efficiencies were compared, the results of these study is shown in the plots below for the four different design configurations. Each SeaWiet design was compared to each NuONE design, for clearer visibility only two design configurations per plot except for the last two plots which show a comparison of all four designs in terms of effective area.

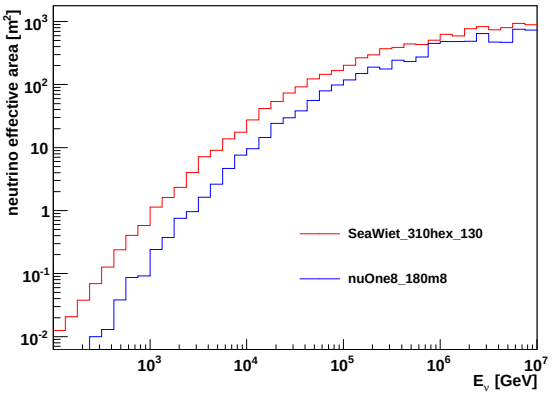

Figure 99: comparison of effective areas, zmod reco algorithm, 2π

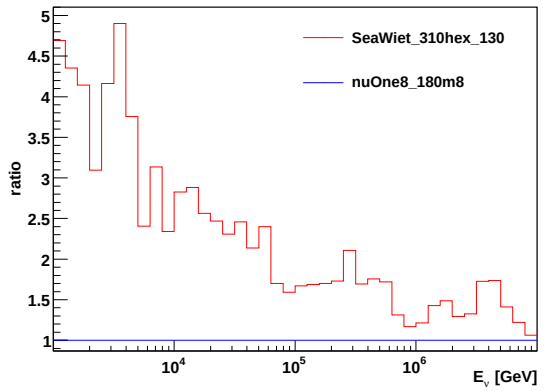

Figure 100: ratio of effective areas, zmod reco algorithm, 2π

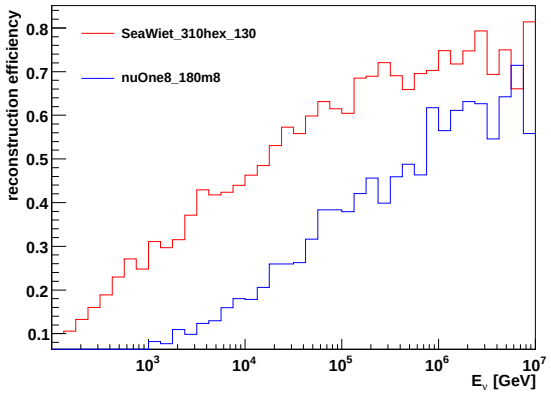

Figure 101: comparison of reconstruction efficiencies, zmod reco algorithm, 2π

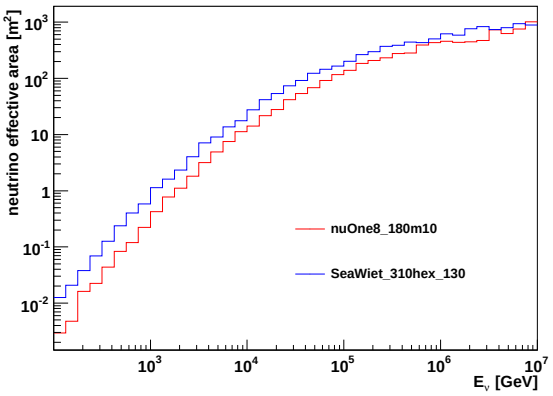

Figure 102: comparison of effective areas, zmod reco algorithm, 2π

The SeaWiet designs yield both a higher effective area as well as a higher reconstruction efficiency. For a neutrino energy of 100 TeV the effective area for all SeaWiet designs is around 50% higher than those of the NuONE designs, which is not a surprise since the SeaWiet detectors are bigger and have a larger total photocathode area, $876.7m^2$ compared to $494.3m^2$. For low energies ($<$ 10 TeV), the effective areas are several times as high as for NuONE while at the high end of the spectrum ($> 10^6 GeV$) the values are still about 10% higher, although here low statistics obfuscate the results somewhat and make it impossible to obtain precise results without using much more data. The reconstruction efficiency at 100 TeV is around 30% higher for SeaWiet than for NuONE (all designs). As will be noted below, this is not just due to the denser instrumentation

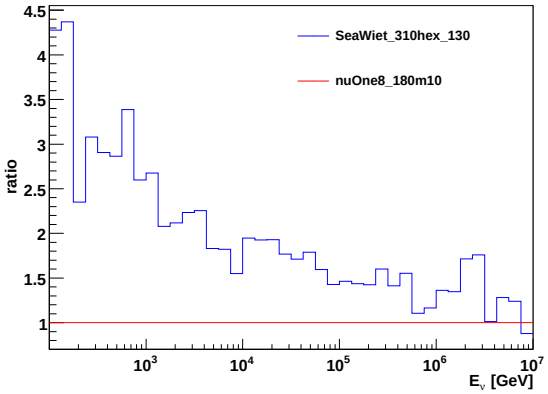

Figure 103: ratio of effective areas, zmod reco algorithm, 2π

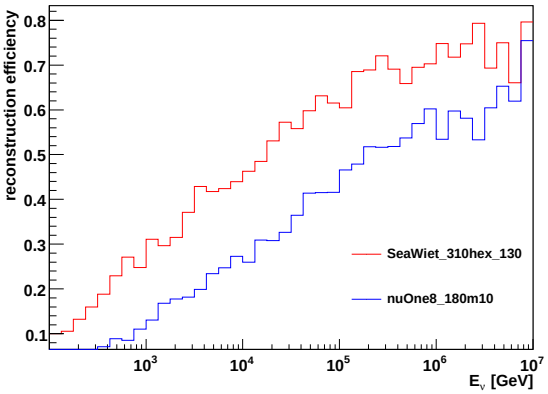

Figure 104: comparison of reconstruction efficiencies, zmod reco algorithm, 2π

of the SeaWiet designs (130m rather than 180m DU distance). At the high end of the energy spectrum, the reconstruction efficiency favours the SeaWiet design even more than the effective area. Here the reconstruction efficiency is still 20% higher than for the NuONE designs. Also, to compare detectors of the same size, the NuONE design with 130m DU distance was used and for the SeaWiet design the 30m storey distance was chosen. For this comparison only results for 4π angular distribution were available. The comparison was done only for the ratio of the reconstruction efficiencies of the two detector configurations since the instrumented volume of the SeaWiet detector is much larger than the compact NuONE detector which would make a comparison of effective areas meaningless.

Even though the NuONE detector features a larger photocathode area per storey than the SeaWiet detector, 1946 cm^2 for NuONE and 1414 $cm2$ for SeaWiet, the SeaWiet design still yields a higher reconstruction efficiency. This excess in reconstruction efficiency is still at 20% in the last energy decade, between 10^6 and 10^7 GeV and higher at

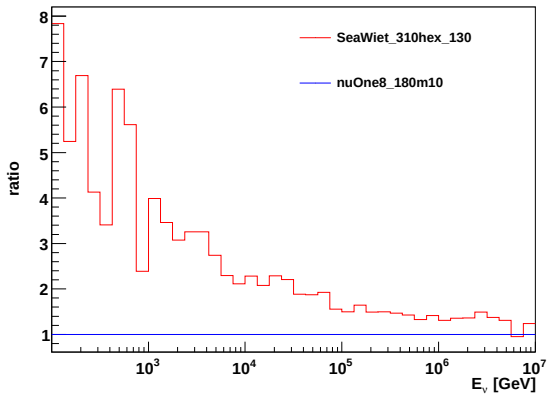

Figure 105: ratio of reconstruction efficiencies, zmod reco algorithm, 2π

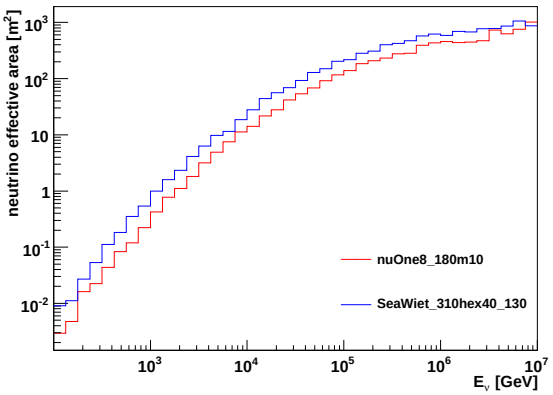

Figure 106: comparison of effective areas, zmod reco algorithm, 2π

lower energies. Considering that both configurations have the same spacial distribution of storeys and that the NuONE storey has a 38% larger photocathode area, this shows clearly that the SeaWiet storey design is superior to the NuONE storey design when it comes to reconstruction efficiency. For the purpose of ascertaining the above mentioned doubling in effective area when using two separate detectors and the fact that a doubling of detection units does not lead to the same effect, a smaller 154 string SeaWiet detector was simulated. Here the resulting effective area of the aforementioned detector is compared to that of the larger, 154 tower configuration on the NuONE detector.

When comparing the design options on the basis of a given number of detection units for both designs, the NuONE detector yields a higher effective area for energies above 10^5 GeV. The SeaWiet detector still reaches on average 80 - 85% of the effective area of the NuONE detector at the higher energies. Due to low statistics, the absolute values especially at both ends of the energy spectrum are to be treated with caution. Since both simulated designs are not canonical only one file of each design was produced. The

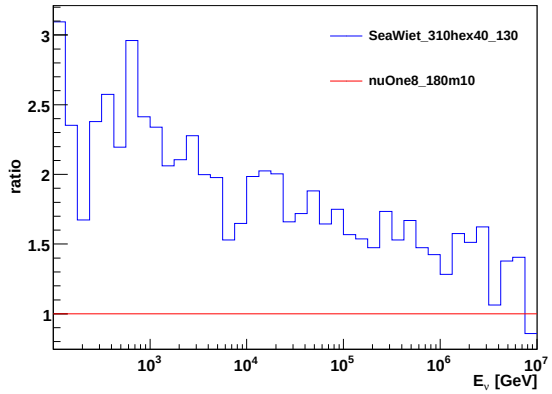

Figure 107: ratio of effective areas, zmod reco algorithm, 2π

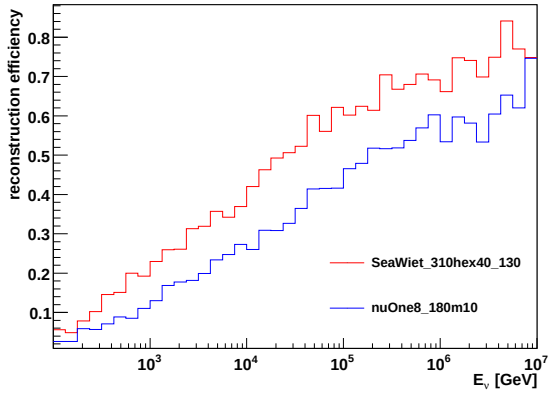

Figure 108: comparison of reconstruction efficiencies, zmod reco algorithm, 2π

denser instrumentation of the SeaWiet detector can nearly compensate for the 38% larger photocathode area in the NuONE design. Additionally, a comparison between the double-sized NuONE detector, two separate detectors to maximise effective area, and a single-sized SeaWiet detector was made. The NuONE detector here is the standard detector with 127 detection units 180m apart featuring 8-inch PMTs, then doubling the effective area, the SeaWiet detector is the 310 hexagonal design with 40m between storeys.

As can be seen from the plots, the SeaWiet detector still performs better in terms of effective area for lower neutrino energies ($< 10^5 GeV$) than even the double-sized NuONE detector. Only in the last energy decade does the double-sized NuONE detector clearly outperform the single-sized SeaWiet detector. Here the SeaWiet detector still achieves an effective area of on average 80% of that of the double NuONE.

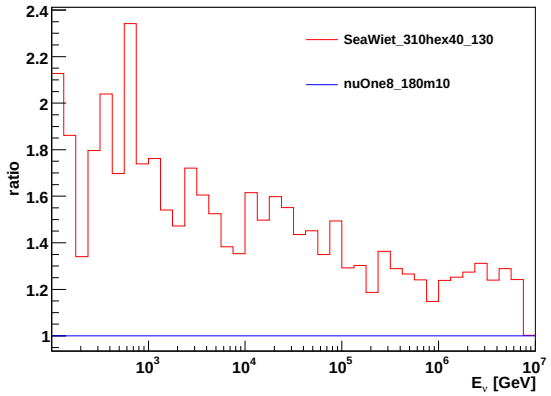

Figure 109: ratio of reconstruction efficiencies, zmod reco algorithm, 2π

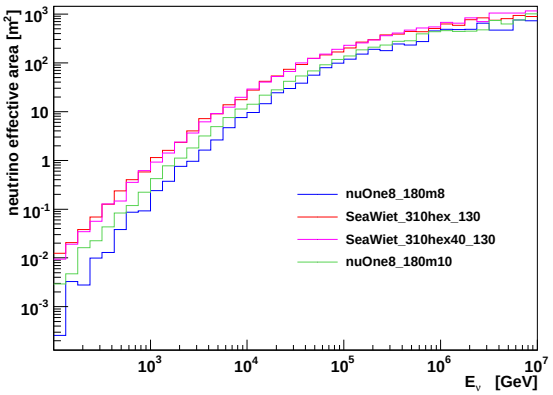

Figure 110: comparison of effective areas, zmod reco algorithm, 2π

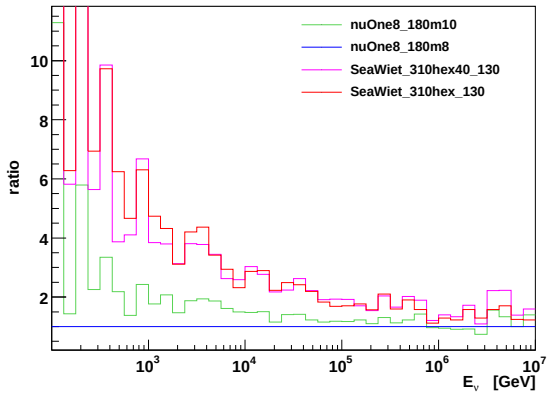

Figure 111: ratio of effective areas, zmod reco algorithm, 2π

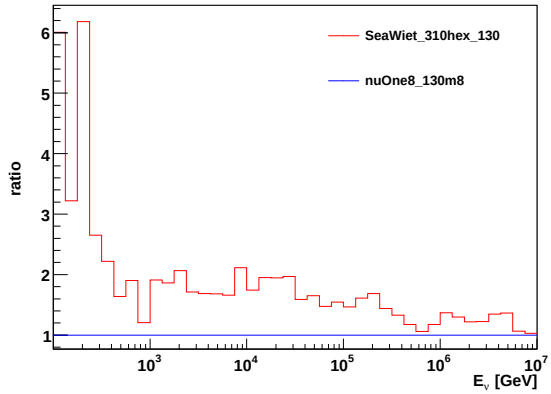

Figure 112: ratio of reconstruction efficiencies, zmod reco algorithm, 2π

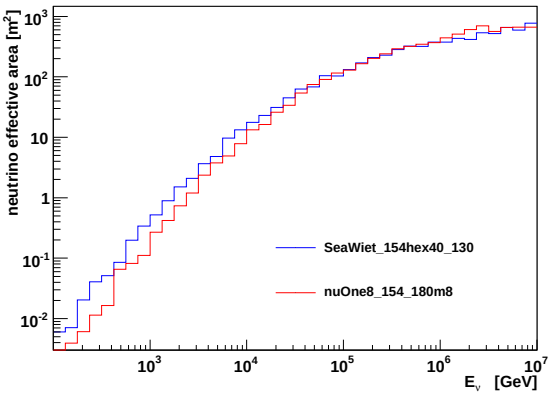

Figure 113: comparison of effective areas, zmod reco algorithm, 2π

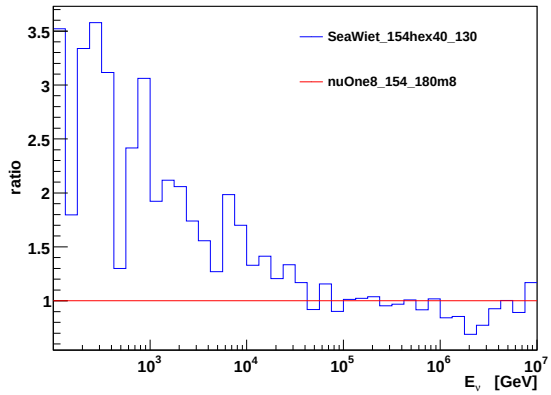

Figure 114: ratio of effective areas, zmod reco algorithm, 2π

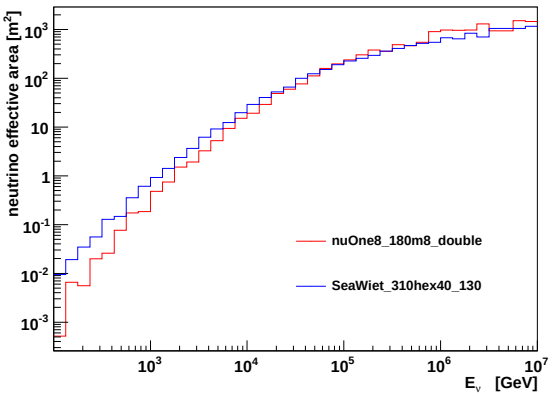

Figure 115: comparison of effective areas, zmod reco algorithm, 2π

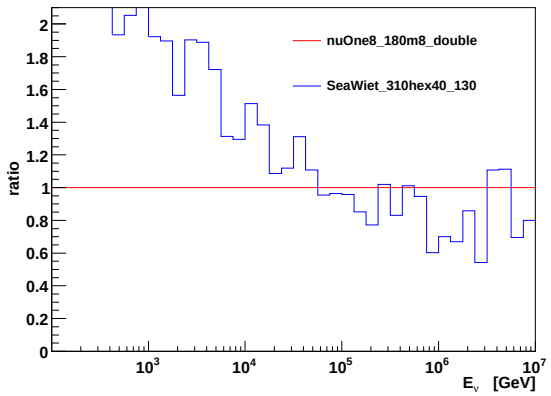

Figure 116: ratio of effective areas, zmod reco algorithm, 2π

9 Conclusion

Regardless of all design considerations, the study has also shown the influence of environmental parameters on the performance of a neutrino telescope. Although a detailed analysis of the effects of the different environmental factors such as absorption length and scattering length is beyond the scope of this study, the results point to some general conclusions. In order to obtain optimal results in terms of reconstruction efficiency and thus effective area, the site should be selected with the largest absorption and scattering lengths. As can be seen from the simulations, the influence of the absorption length is far greater than that of the scattering length for which even when increased by 450% results in increase of effective area of only around 10As for the depth of the site, the analysis for the SeaWiet detector shows that going 1000m deeper, from 3500m to 4500m, reduces the atmospheric muon background by 75%, clearly showing that greater sea depths are prferable. However, it has yet to be determined if this reduction in background has such a great effect as to justify the engineering challanges that are incurred when moving the detector to a deeper site, which is usually farther away from the shore. The actual impact beyond measuring the background rates of the atmospheric muon background on the detector performance has not been studied thoroughly in this analysis. The ^{40}K background also plays only a limited role in this study. As the variation of this background rate had only a relatively miniscule effect on the detector performance, a search for a site with low salinity is not worth the effort. A far bigger role can be expected for the bioluminesance background which has not been studied in this analysis. To sum up the considerations of the environmental parameters, the ideal site for KM3NeT is a deep sea location with extremely clear water and a complete lack of marine life that is closely to the shore. This study cannot give an answer as to which actual location this might be. The superior performance of the multi-PMT-equipped SeaWiet design in terms of neutrino effective area is the result of several factors. The detector design contains a larger photocathode area than the NuONE design, $876.7m^2$ compared to $494.3m^2$. The larger detector volume results in a larger portion of the generation volume filled with instrumentation. Since the generation volume is calculated from the centre of gravity (c.o.g.) of the detector, the generation volume is the same for all design configurations. This leads to a direct increase in reconstruction capability if the detector volume is increased. Also the coverage of the OM with PMTs is nearly homogeneous in case of SeaWiet while the double PMT optical module offers a smaller angular acceptance. An additional effect of this homogeneous coverage is the availability of upward-looking PMTs which allows the detection of photons that would go unnoticed in a nuOne storey where they would hit the upper, blind half of the OM in case of the central downward-looking PMTs or the inner blind half of the outward-looking PMTs. With the multi-PMT module hits on neighbouring storeys are therefore more likely, especially for low-energy events which produce few photons that might be able to hit the outward-looking PMTs on the nuOne storey. Both of these effects result in a higher reconstruction efficiency for SeaWiet since the reconstruction algorithms depend on a certain minimum number of hits to be successful. Not only provides the SeaWiet design a denser instrumentation and overall angular acceptance of the optical module, but the composition of the OM of multiple photomultipliers allows for a far higher probability of multiple hits on one storey. A number of photons that would have hit only a single large, i.e. 8-inch, PMT can hit

several small PMTs. If this hits occur within a smaller time window than the phototube needs to recover from a hit, which would be counted as one hit in the large PMT but can be resolved in the multi-PMT OM and identified as an L1 hit even if each hit would have measured with a lower amplitude than required for a big hit for the 8-inch PMT when combined. This increase in reconstruction efficiency is most clearly visible in the comparison of the two configuration with the same spacial distribution of storeys, where the distribution of photocathode area even outweights the 38% larger photocathode area of the NuONE storey. These effects do also increase vulnerability to the ^{40}K background (also to bioluminesence which is neglected here) but the results show that the gain in reconstruction efficiency does outweight the increase in background. However further studies are currently performed into the calculations of false coincidences caused by ^{40}K background hits in multi-OMs. Preliminary results show a rate of ca. 700 Hz of correlated hits when the decays occur close to the optical module (several metres)[18].

The reconstruction efficieny could be further increased by a combination of the multi-OM storey and the extended structure. This would increase the photocathode area per storey and could reduce the number of false coincidences by rejecting low-energy hits in one OM only while still being able to use the coincident hits from two or more OMs within the same storey. Preliminary studies show promising results [**?**]. Work on this convergence of the two design options was begun as part of this study but the ANTARES software chain is in its current form unable to handle more than 60 PMTs per storey, with the exception of the latest prototype genhen version (not used in this study). To accomodate a higher number of PMTs the entire software chain has to be modified, including some of the libraries neccessary for the compilation of all seperate programs. The modifications suggested by Sebastian Kuch are not nearly extensive enough. Only gendet works without any alterations and genhen has been successfully recompiled to handle 62 PMTs per storey. Beyond that point (km3, reco) all attempts so far have failed. For further analyses it is necessary to focus on fewer design configurations to allow for a significant increase in data to avoid the pitfalls of low statistics. It may also be more feasable to abandone the ANTARES software chain in favour of the SeaTray framework and start from scratch. Apart from any future considerations, the result of this study shows that when using the neutrino effective area as a measure of performance, the SeaWiet design with its multi-PMT storeys is better than the NuONE design. Especially the comparison between the design configurations with the same spacial distribution shows that even with a higher photocathode area per storey, the NuONE detector still has a lower reconstruction efficiency. Even when compared to a double-sized NuONE detector the SeaWiet detector reaches 80% of the combined effective area. This does not include any assumptions of other detector parameters or engineering and budgetal constraints, so this study cannot give a final answer to the question which detector design is the best option for KM3NeT.

References

[1] F.Bernard (2000), *Caractrisation des performances d un tlescope sous-marin neutrinos pour la detection de cascades contenues dans le cadre du projet ANTARES. PhD thesis Universite de la Mediterrane, Aix-Marseille II, Marseille, France (2000)*

[2] http://www.icecube.wisc.edu

[3] http://www.antares.in2p3.fr

[4] http://www.km3net.org (2008)

[5] http://www.km3net.org (2008)

[6] P.Kooijman et al. (2008), *KM3NeT Conceptual Design Report for a Deep-Sea Research Infrastructure in the Mediterranean Incorporating a Very Large Volume Neutrino Telescope,ISBN 978-90-6488-031-5*

[7] not specified (2009), *νONE Obeservatory of Neutrino Events*

[8] not specified (2009), *SeaWiet SEnsor Architecture for a WIde Energy range Telescope*

[9] O.Kavatsyuk (2009), *Photo-Sensors for a Multi-PMT Optical Module in KM3NeT, VLVNT09 contribution*

[10] S.Anvar et al. (2009), *MEDUSA MEDiterranean Undersea String Architecture*

[11] F.Cassol Brunner (2000), *ANTARES-Soft/2000-008*

[12] D.Bailey (2002) , *ANTARES-Soft/2002-004*

[13] S.Navas et al. (1999), *ANTARES-Soft/1999-011*

[14] A.Heijboer (2002), *ANTARES-Soft/2002-002*

[15] D.Zaborov (2004), *ANTARES-Soft/2004-004*

[16] G. Carminati (2007), *ANTARES-Soft/2007-004*

[17] http://wiki.km3net.physik.uni-erlangen.de

[18] B. Herold (2009), *K 40 Background Simulations for the SeaWiet OM, VLVNT09 contribution*

[19] A. Tsirigotis (2009), *Using HOURS to evaluate KM3NeT designs, VLVNT09 contribution*

List of Figures

Acknowledgements

I would like to thank everyone who helped with my work and who made ECAP a place where work does not feel like work.
I would especially like to thank Uli Katz, Rezo Shanidze and Björn Herold for their help above and beyond the call of duty.